
VACA: DESIGN OF VARIATIONAL GRAPH AUTOENCODERS FOR INTERVENTIONAL AND COUNTERFACTUAL QUERIES

Pablo Sanchez-Martin*

Max Planck Institute for Intelligent Systems
Tübingen, Germany
pablo.sanchez-martin@tuebingen.mpg.de

Miriam Rateike*

Max Planck Institute for Intelligent Systems
Tübingen, Germany
mrateike@tuebingen.mpg.de

Isabel Valera

Saarland University
Saarbücken, Germany
ivalera@cs.uni-saarland.de

ABSTRACT

In this paper, we introduce VACA, a novel class of variational graph autoencoders for causal inference in the absence of hidden confounders, when only observational data and the causal graph are available. Without making any parametric assumptions, VACA mimics the necessary properties of a *Structural Causal Model* (SCM) to provide a flexible and practical framework for approximating interventions (*do-operator*) and *abduction-action-prediction* steps. As a result, and as shown by our empirical results, VACA accurately approximates the interventional and counterfactual distributions on diverse SCMs. Finally, we apply VACA to evaluate counterfactual fairness in fair classification problems, as well as to learn fair classifiers without compromising performance.

Keywords Graph Neural Network · Causality · Counterfactual · Intervention · Variational Autoencoder

1 Introduction

Graph Neural Networks (GNNs) are a powerful tool for graph representation learning and have been proven to excel in practical complex problems like neural machine translation [1], traffic forecasting [5, 47], or drug discovery [11].

In this work, we investigate to which extent the inductive bias of GNNs—encoding the causal graph information—can be exploited to answer interventional and counterfactual queries. More specifically, to approximate the interventional and counterfactual distributions induced by interventions on a causal model. To this end, we assume i) causal sufficiency—i.e., absence of hidden confounders; and, ii) access to observational data and the true causal graph. We stress that the causal graph can often be inferred from expert knowledge [52] or via one of the approaches for causal discovery [12, 42]. With this analysis we aim to complement the concurrent line of research that theoretically studies the use of Neural Networks (NN) [45], and more recently GNNs [49], for causal inference.

To this end, we describe the architectural design conditions that a variational graph autoencoder (VGAE)—as a density estimator that leverages a priori graph structure—must fulfill so that it can approximate causal interventions (*do-operator*) and *abduction-action-prediction* steps [33]. The resulting Variational Causal Graph Autoencoder, referred to as VACA, enables *approximating* the observational, interventional and counterfactual distributions induced by a causal model with unknown structural equations. We remark that parametric assumptions on the structural causal equations are in general not testable, may thus not hold in practice [34] and may lead to inaccurate results, if misspecified. VACA addresses this limitation by including uncertainty, i.e., a probabilistic model, in the estimation of the causal-parent relationships.

*Equal contribution

We show in extensive synthetic experiments that VACA outperforms competing methods [16, 17] on complex datasets at estimating not only the mean of the interventional/counterfactual distribution (as in previous work), but also the overall distribution (measured in terms of Maximum Mean Discrepancy [13]). Finally, we show a practical use-case in which VACA is used to assess counterfactual fairness of different classifiers trained on the real-world German Credit dataset [7], as well as to learn counterfactually fair classifiers without compromising performance.

1.1 Related Work

Deep generative models are enjoying increasing attention for causal queries in complex data [26, 28]. Existing approaches for causal inference focus on i) estimating the Average Treatment Effect (ATE)—a specific type of group-level causal queries—by assuming a fixed causal graph that includes a treatment variable [18, 25, 36, 39, 43, 50]; ii) discovering and intervening on the causal latent structure of the (e.g., image) data [18, 28, 30, 40, 46]; or iii) addressing interventional and/or counterfactual queries by fitting a conditional model for each observed variable given its causal parents [10, 16, 21, 29, 31].

Within the scope of causality, GNNs have predominantly been used for causal discovery [48, 51] and only very recently, concurrent with us, exploited to answer interventional queries [49].

Khemakhem et al. [17] propose CAREFL, an autoregressive normalizing flow for both causal discovery and inference. The authors focus on (multi-dimensional) bi-variate graphs, but their approach can be extended to more general directed acyclic graphs (DAGs) using e.g., neuronal spline flows [8]. However, causal assumptions in a graph are modeled not only by the direction of edges, but also the absence of edges [32]. For the task of causal inference CAREFL is unable to exploit the absence of edges fully as it reduces a causal graph to its causal ordering (which may not be unique). Further, the authors only evaluate interventions in root nodes (which reduces to conditioning on the intervened-upon variable).

Karimi et al. [16] answer interventional queries by fitting a conditional variational autoencoder (CVAE) to each conditional in the Markov factorization implied by the causal graph. As each observed variable is independently fitted, the mismatch between the true and generated distribution can cause errors that propagate to the distribution of its descendants. This can be problematic, especially for long causal paths. Pawlowski et al. [31] propose an approach similar to Karimi et al. [16], and additionally propose an approach based on normalizing flows to approximate the causal parent-child effect.

In contrast, VACA leverages i) GNNs to encode the causal graph information (inductive bias), ii) the GNN message passing algorithm to approximate the effect of interventions (*do-operator* [33]) in the causal graph, and iii) jointly optimizes the observational distribution for all observed variables to avoid error propagation along the Markov factorization. We thoroughly evaluate the performance of VACA and compare it with related work, at approximating both interventional and counterfactual distributions induced by interventions on both root and non-root nodes in a wide variety of causal models.

2 Background

In this section, we first provide a brief overview on SCMs and then introduce the main building block of VACA, i.e., variational graph autoencoders.

2.1 Structural causal models

An SCM $\mathcal{M} = (p(\mathbf{U}), \tilde{\mathbf{F}})$ determines how a set of d endogenous (observed) random variables $\mathbf{X} := \{X_1, \dots, X_d\}$ is generated from a set of exogenous (unobserved) random variables $\mathbf{U} := \{U_1, \dots, U_d\}$ with prior distribution $p(\mathbf{U})$ via the set of *structural equations* $\tilde{\mathbf{F}} = \{X_i := \tilde{f}_i(\mathbf{X}_{\text{pa}(i)}, U_i)\}_{i=1}^d$. Here $\mathbf{X}_{\text{pa}(i)}$ refers to the set of variables directly causing X_i , i.e., parents of i . Similarly to [16, 17, 32], we consider SCMs that are associated with a directed acyclic *causal graph* (although Section 4.4 relaxes this assumption). We here denote the causal graph by $\mathcal{G} := (\mathcal{V}, \mathcal{E})$, where each node $i \in \mathcal{V}$ corresponds to an endogenous variable X_i . The set of directed edges $(j, i) \in \mathcal{E}$ represent the causal parent-child relationship between endogenous variables [32], i.e. X_j is a parent of X_i . \mathcal{E} can be represented by the adjacency matrix $\mathbf{A} \in \{0, 1\}^{d \times d}$, such that $A_{ij} = 1$ if $(j, i) \in \mathcal{E}$ and $A_{ij} = 0$, otherwise. We also define the set of neighbors, a.k.a. parents, of node i as $\text{pa}(i) = \mathcal{N}_i = \{j\}_{(j,i) \in \mathcal{E}}$ and $\text{pa}^*(i) := \text{pa}(i) \cup i$. Given an SCM, there are two types of causal queries of general interest: interventional queries, e.g., “What would happen to the population \mathbf{X} , if variable X_i would be set to a fixed value α ?”, and counterfactual queries, e.g., “What would have happened to a specific factual sample \mathbf{x}^F , had X_i been set to a value α ?”. In more detail, *interventional queries* aim to evaluate the effect at the population level (*run* 2) of a specific intervention on, or equivalently manipulations of, a subset of the endogenous variables $\mathcal{I} \subseteq [d] := \{1, \dots, d\}$. Interventions on an SCM \mathcal{M} are often represented with the *do-operator*

$do(X_i = \alpha_i)$ [33] and lead to a modified SCM $\mathcal{M}^{\mathcal{I}}$ which induces a new distribution over the set of endogenous variables $p(\mathbf{X} \mid do(X_i = \alpha_i))$, which is referred to as the *interventional distribution*. In \mathcal{G} an intervention removes incoming edges to node i and sets $X_i = \alpha$ (see Figure 1b). A *counterfactual query* for a given factual instance \mathbf{x}^F aims to estimate what would have happened had $\mathbf{X}_{\mathcal{I}}$ instead taken value α . This effect is captured by the *counterfactual distribution* $p(\mathbf{x}^{CF} \mid \mathbf{x}^F, do(X_{\mathcal{I}} = \alpha))$, which can be computed using the *abduction-action-prediction* procedure by Pearl [33]. Refer to Section 3 for further details on the computation of the interventional and counterfactual distributions within our framework.



Figure 1: *triangle* SCM $\mathcal{M} = \{p(\mathbf{U}), \tilde{\mathbf{F}}\}$, $\mathbf{U} \sim p(\mathbf{U})$ with $d = |\mathbf{X}| = 3$ endogenous variables where $X_1 := \tilde{f}_1(U_1)$, $X_2 := \tilde{f}_2(X_1, U_2)$, $X_3 := \tilde{f}_3(X_1, X_2, U_3)$ with (a) the corresponding causal graph \mathcal{G} and (b) the causal graph corresponding to $\mathcal{M}^{\mathcal{I}}$ after intervention $do(X_2 = \alpha)$. Blue (red) arrows highlight the direct (indirect) causal path from X_1 to X_3 (via X_2).

2.2 Variational Graph Autoencoder and Graph Neural Networks

Variational Autoencoders (VAEs). VAEs [19] are powerful latent variable models based on neural networks (NNs) for jointly i) learning expressive density estimators $p(\mathbf{X}) \approx \int p_{\theta}(\mathbf{X} \mid \mathbf{Z})p(\mathbf{Z})d\mathbf{Z}$, where the likelihood function (a.k.a. *decoder*) is parameterized using a NN with parameters θ , and ii) performing approximate posterior inference over the latent variables \mathbf{Z} made possible via a variational distribution (a.k.a. *encoder*) $q_{\phi}(\mathbf{Z} \mid \mathbf{X})$ parameterized using a NN with parameters ϕ . The parameters θ and ϕ can be learned by maximizing a lower bound on the log-evidence [2, 27, 35, 41].

Variational Graph Autoencoders (VGAEs). Kipf and Welling [20] extend VAEs to account for prior graph structure information on the data [48]. VGAEs define a (potentially multidimensional) latent variable Z_i per observed variable X_i , i.e., $\mathbf{Z} := \{Z_1, \dots, Z_d\}$. Additionally, VGAEs rely on an adjacency matrix \mathbf{A} , which is used by two GNNs, one for the encoder and one for the decoder, to enforce structure on the posterior approximation $q_{\phi}(\mathbf{Z} \mid \mathbf{X}, \mathbf{A})$ and the likelihood $p_{\theta}(\mathbf{X} \mid \mathbf{Z}, \mathbf{A})$. Hence, \mathbf{A} —given as prior—determines which variables X_i influence $Z_j \forall i, j \in [d]$.

Graph Neural Networks (GNNs). In its most general form, a GNN is a composition of message passing layers [11], where each layer updates the state of each node in \mathcal{G} . In particular, the state of node i at the output of layer l , i.e., \mathbf{h}_i^l , is specified as:

$$\mathbf{h}_i^l = f^u(\mathbf{h}_i^{l-1}, f^a(\{\mathbf{m}_{ij}^l\}_{j \in \mathcal{N}_i}); \theta_u^l). \quad (1)$$

First, node i receives a message $\mathbf{m}_{ij}^l = f^m(\mathbf{h}_i^{l-1}, \mathbf{h}_j^{l-1}; \theta_m^l)$ from each of its neighbors $j \in \mathcal{N}_i$. Then, these messages are aggregated via f^a . Finally, \mathbf{h}_i^l is computed as a function f^u of the node’s previous state \mathbf{h}_i^{l-1} and the aggregated message. Note, if a GNN has N_h hidden layers, then the output for node i depends not only on its direct neighbors \mathcal{N}_i , but also on its neighbors up to order $N_h + 1$ (hops). For example, if $N_h = 0$ ($N_h = 1$) then the output for each node only depend on its direct neighbors, i.e., *parents* (2-hop neighbors, i.e., *grand-parents*). For a detailed description of GNNs, please refer to Appendix A.

3 Observational, interventional and counterfactual distributions

In this section, we introduce the observational, interventional and counterfactual distributions (triggered by any intervention of the form $do(\mathbf{X}_{\mathcal{I}} = \alpha)$) that are induced by an SCM $\mathcal{M} = \{p(\mathbf{U}), \tilde{\mathbf{F}}\}$. Specifically, we summarize the main properties of an SCM that will allow us to propose a novel class of VGAEs, namely VACA, to compute accurate estimates of these distributions using observational data and a known causal graph. To this end, we assume the absence of hidden confounders, i.e., we assume that $p(\mathbf{U}) = \prod_{i=1}^d p(U_i)$.

Observational distribution. The SCM \mathcal{M} determines the observational distribution $p(\mathbf{X})$ over the set of endogenous variables $\mathbf{X} = \{X_1, \dots, X_d\}$, which satisfies causal factorization [38], i.e., $p(\mathbf{X}) = \prod_{i=1}^d p(X_i \mid \mathbf{X}_{\text{pa}(i)})$. That is, after marginalizing out the exogenous variables \mathbf{U} , the distribution of each endogenous variable X_i depends only on its parents, i.e., $\mathbf{X}_{\text{pa}(i)}$.

The *observational distribution* can alternatively be written only in terms of the exogenous variables \mathbf{U} as

$$p(\mathbf{X}) = \mathbf{F}_{\#}[p(\mathbf{U})], \quad (2)$$

i.e., $p(\mathbf{X})$ is the pushforward of $P(\mathbf{U})$ through \mathbf{F} . Here $\mathbf{F} : \mathbf{U} \rightarrow \mathbf{X}$ corresponds to the set of structural equations, which directly transform the exogenous variables \mathbf{U} into the endogenous variables \mathbf{X} . This is equivalent to $\tilde{\mathbf{F}}$, which takes as input both the exogenous variable and the parent (endogenous) variables of a target endogenous variables to compute its value.

Let us denote by $\text{an}(i)$ the set of indexes of the ancestors of i , and $\text{an}^*(i) := \text{an}(i) \cup \{i\}$. Then, the causal factorization induced by \mathcal{M} leads to the following property of $\mathbf{F}(\mathbf{U})$:

Property 1. *Each endogenous variable X_i can be expressed as a function of its exogenous variable U_i and the ones of all its causal ancestors, i.e., $\mathbf{F}(\mathbf{U}) = \{X_i = f_i(\{U_j\}_{j \in \text{an}^*(i)})\}$. This, together with the causal sufficiency assumption, implies that X_i is statistically independent of $U_j, \forall j \notin \text{an}^*(i)$.*

Interventional distribution. As stated in Section 2.1, interventions on a set of variables \mathcal{I} can be performed using the *do-operator*, which can be seen as a mapping $\text{do}(\mathbf{X}_{\mathcal{I}} = \alpha) : \mathcal{M} \mapsto \mathcal{M}^{\mathcal{I}} = (p(\mathbf{U}), \tilde{\mathbf{F}}^{\mathcal{I}})$ where $\tilde{\mathbf{F}}^{\mathcal{I}} = \{\tilde{f}_i\}_{i \notin \mathcal{I}} \cup \{\alpha_i\}_{i \in \mathcal{I}}$. As above, we can represent the resulting set of *intervened structural equations* as $\mathbf{F}^{\mathcal{I}} = \{f_i\}_{i \notin \mathcal{I}} \cup \{\alpha_i\}_{i \in \mathcal{I}}$, and thus write the *interventional distribution* as:

$$p(\mathbf{X} \mid \text{do}(\mathbf{X}_{\mathcal{I}} = \alpha)) = \mathbf{F}^{\mathcal{I}}_{\#}[p(\mathbf{U})]. \quad (3)$$

Property 2. *After an intervention $\text{do}(\mathbf{X}_{\mathcal{I}} = \alpha)$ on \mathcal{M} , all the causal paths from $U_j \forall j \in \text{an}^*(i)$ to X_i that include an intervened-upon variable in $\mathbf{X}_{\mathcal{I}}$ (i.e., the causal paths where $\mathbf{X}_{\mathcal{I}}$ is a mediator) are severed in $\mathbf{F}^{\mathcal{I}}$, while the rest of causal paths remain untouched.*

The above property is illustrated in Figure 1, where we can observe that after an intervention $\text{do}(X_2 = \alpha)$, the indirect causal path (in red) from X_1 , and thus from U_1 , to X_3 via X_2 is severed, while the direct path (in blue) remains.

Counterfactual distribution. Assuming the SCM $\mathcal{M} = \{p(\mathbf{U}), \tilde{\mathbf{F}}\}$ to be known, the following three steps defined by Pearl [32] allow to compute counterfactuals \mathbf{x}^{CF} : i) *Abduction*: infer the values of the exogenous variables \mathbf{U} for a factual sample \mathbf{x}^F , i.e., compute $p(\mathbf{U} \mid \mathbf{x}^F)$; ii) *Action*: intervene with $\text{do}(\mathbf{X}_{\mathcal{I}} = \alpha) : \mathcal{M} \mapsto \mathcal{M}^{\mathcal{I}} = (p(\mathbf{U}), \tilde{\mathbf{F}}^{\mathcal{I}})$; and iii) *Prediction*: use the posterior distribution $p(\mathbf{U} \mid \mathbf{x}^F)$ and the new structural equations $\tilde{\mathbf{F}}^{\mathcal{I}}$ to compute $p(\mathbf{x}^{CF} \mid \mathbf{x}^F)$. The prediction step can alternatively be computed using the new set of structural equations $\mathbf{F}^{\mathcal{I}}$ defined in terms of the exogenous variables \mathbf{U} , so that we can write the *counterfactual distribution* as:

$$p(\mathbf{x}^{CF} \mid \mathbf{x}^F, \text{do}(\mathbf{X}_{\mathcal{I}} = \alpha)) = \mathbf{F}^{\mathcal{I}}_{\#}[p(\mathbf{U} \mid \mathbf{x}^F)]. \quad (4)$$

Importantly, the posterior distribution $p(\mathbf{U} \mid \mathbf{x}^F)$ satisfies:

Property 3. *In the abduction step, statistical independence implies that conditioned on the endogenous variables of the factual sample \mathbf{x}^F , each exogenous variable U_i is independent of the factual value x_j^F if $j \neq i$ and the variable X_j is not a parent of X_i , i.e., $j \notin \text{pa}^*(i)$.*

4 Variational Causal Autoencoder (VACA)

In this section, we present a novel variational causal graph autoencoder (VACA) to approximate the observational (2), interventional (3) and counterfactual (4) distributions. While the underlying SCM \mathcal{M} is unknown, we assume access to the true causal graph \mathcal{G} and observational data $\{\mathbf{x}_n\}_{n=1}^N$, i.e., i.i.d. samples of the observational distribution induced by \mathcal{M} (in the absence of hidden confounders).

Definition 4.1. (VACA). *Given a causal graph \mathcal{G} over a set of endogenous variables $\mathbf{X} = \{X_1, \dots, X_d\}$, which establishes the set of parents $\text{pa}(i)$ for each variable X_i (including the i -th node), VACA is defined by:*

- A causal adjacency matrix \mathbf{A} , which is a $d \times d$ binary matrix with elements $A_{ij} = 1$ if $j \in \text{pa}^*(i)$, i.e., when $i = j$ or j is a parent of i . Otherwise, $A_{ij} = 0$.
- A prior distribution $p(\mathbf{Z}) = \prod_i p(Z_i)$ over the set of latent variables $\mathbf{Z} = \{Z_1, \dots, Z_d\}$.
- A decoder $p_{\theta}(\mathbf{X} \mid \mathbf{Z}, \mathbf{A})$, which is a GNN (parameterized by θ) that takes as input the set of latent variables \mathbf{Z} and the causal adjacency matrix \mathbf{A} , and outputs the parameters of the likelihood $p_{\theta}(\mathbf{X} \mid \mathbf{Z}, \mathbf{A})$.
- An encoder $q_{\phi}(\mathbf{Z} \mid \mathbf{X}, \mathbf{A})$, which is a GNN (parameterized by ϕ) that takes as input the endogenous variables \mathbf{X} and the causal adjacency matrix \mathbf{A} , and outputs the parameters of the posterior approximation $q_{\phi}(\mathbf{Z} \mid \mathbf{X}, \mathbf{A})$.

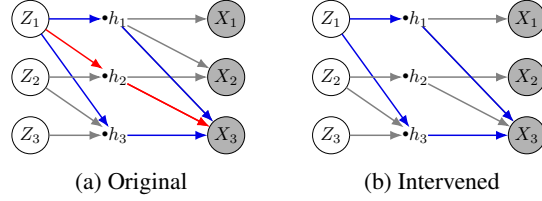


Figure 2: VACA decoder (a) with and (b) without intervening on X_2 . Message passing in the GNN correspond to direct (blue) and indirect (red) causal paths in Figure 1.

Next, we discuss how to design VACA such that it is able to capture the observational, interventional, and counterfactual distribution induced by an unknown SCM. Importantly, we derive the necessary conditions on the design of both the encoder and decoder GNNs such that VACA can mimic the SCM properties introduced in Section 3.

4.1 Observational distribution

VACA approximates the *observational distribution* in (2) using the generative model as

$$p(\mathbf{X}) \approx \int p_\theta(\mathbf{X} \mid \mathbf{Z}, \mathbf{A})p(\mathbf{Z})d\mathbf{Z}, \quad (5)$$

where $p_\theta(\mathbf{X} \mid \mathbf{Z}, \mathbf{A}) = \prod_{i=1}^d p_\theta(X_i \mid \mathbf{Z}, \mathbf{A})$. Figure 3a depicts this generative process.

Relationship between \mathbf{Z} and \mathbf{U} . When comparing (5) with the true observational distribution in (2), we observe that the latent variables \mathbf{Z} play a similar role to the exogenous variables \mathbf{U} , and the decoder $p_\theta(\mathbf{X} \mid \mathbf{Z}, \mathbf{A})$ plays a similar role to the structural equations \mathbf{F} . We remark that \mathbf{Z} do not need to correspond to the true exogenous variables (i.e., $p(\mathbf{U}) \neq p(\mathbf{Z})$), and thus, the decoder does not aim to approximate the causal structural equations. Yet, we assume that there is one independent latent variable Z_i for every observed variable X_i capturing all the information of X_i that cannot be explained by its parents. Thus, since X_i is in turn a (deterministic) function of its parents $\text{pa}(i)$ and its exogenous variable U_i , the posterior $p(Z_i \mid X_i, \text{pa}(i))$ aims to capture the information that U_i contributes to X_i (i.e., the information of X_i not contributed by its parents). That is—similar to $p(U_i \mid X_i, \text{pa}(i))$, the (true) posterior distribution— $p(Z_i \mid X_i, \text{pa}(i))$ should depend only on X_i and parents $\text{pa}(i)$.

Observational noise. VACA has observational noise that is not present in the true SCM, where an observed variable is assumed to be a deterministic transformation of its exogenous variables and parents via the structural equations (SEs). As VACA does not have access to the true SEs (nor to the true distribution of the exogenous variables), the *noise* of the likelihood $p_\theta(\mathbf{X} \mid \mathbf{Z}, \mathbf{A})$ can be interpreted as an estimate of the uncertainty on the estimated observational distribution (due to the uncertainty on the true SCM).

Here, we seek to ensure that the $p(\mathbf{X})$ induced by VACA complies with causal factorization (**Property 1** in Section 3). To that end, the design of the decoder GNN must assure that $p_\theta(X_i \mid \mathbf{Z}, \mathbf{A}) = p_\theta(X_i \mid \mathbf{Z}_{\text{an}^*(i)})$. That is, that X_i depends only on Z_j if $j = i$ or X_j is an ancestor of X_i in the causal graph.

Proposition 1. (Causal factorization). *VACA satisfies causal factorization, $p_\theta(\mathbf{X} \mid \mathbf{Z}, \mathbf{A}) = \prod_i p_{\theta_i}(X_i \mid \mathbf{Z}_{\text{an}^*(i)})$, if and only if the number of hidden layers in the decoder is greater or equal than $\delta - 1$, with δ being the length of the longest shortest path between any two endogenous nodes.*

The above proposition (proved in Appendix B) is based on the fact that, in a GNN with N_h hidden layers (and $N_h + 1$ layers in total), the output for the i -th node depends on its neighbors of up to $N_h + 1$ hops. As an example, consider the following *chain* causal graph: $X_1 \rightarrow X_2 \rightarrow X_3$, such that $\delta = 2$. In the decoder, the first layer yields a hidden representation for the 3-rd node $h_3^1 := f(f(Z_2), Z_3)$ that only depends on Z_2 and Z_3 . Thus, we need a second layer for its output $h_3^2 := f(h_3^1, Z_3) = f(f(f(Z_1), Z_2), Z_3)$ to depend on Z_1 (note that X_1 is an ancestor of X_3).

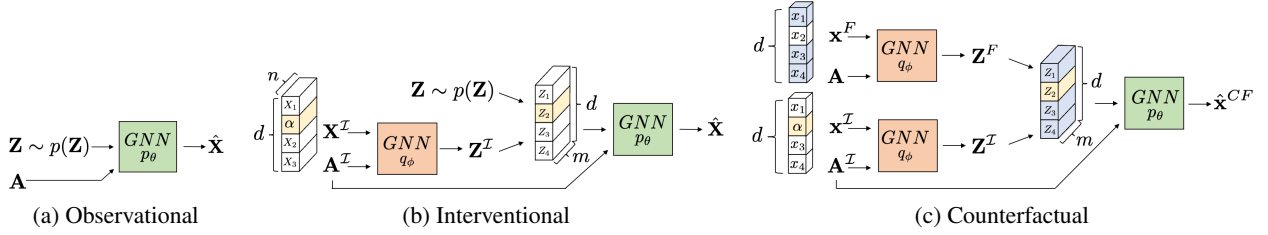


Figure 3: VACA generation of (a) observational, (b) interventional, and (c) counterfactual samples. The ‘hat’ in $\hat{\mathbf{X}}$ and $\hat{\mathbf{x}}^{CF}$ indicates that they are sample estimates of the true random variables.

4.2 Interventional distribution

VACA approximates the *interventional distribution* in (3) as (illustrated in Figure 2):

$$p(\mathbf{X} \mid do(\mathbf{X}_{\mathcal{I}} = \boldsymbol{\alpha})) \approx \int \int p_{\theta}(\mathbf{X} \mid \tilde{\mathbf{Z}}, \tilde{\mathbf{Z}}^{\mathcal{I}}, \mathbf{A}^{\mathcal{I}}) p(\tilde{\mathbf{Z}}) q_{\phi}(\tilde{\mathbf{Z}}^{\mathcal{I}} \mid \mathbf{A}^{\mathcal{I}}, \mathbf{X}_{\mathcal{I}}) d\tilde{\mathbf{Z}} d\tilde{\mathbf{Z}}^{\mathcal{I}}, \quad (6)$$

where $\tilde{\mathbf{Z}}^{\mathcal{I}} = \{Z_i^{\mathcal{I}}\}_{i \in \mathcal{I}}$ is the subset of latent variables associated with the intervened-upon variables $\mathbf{X}_{\mathcal{I}}$, and $\tilde{\mathbf{Z}} = \{Z_i\}_{i \notin \mathcal{I}}$ denotes the subset of latent variables associated with the rest of the observed variables. Importantly, here the *do-operator* is performed on the causal adjacency matrix as $do(\mathbf{X}_{\mathcal{I}} = \boldsymbol{\alpha}) : \mathbf{A} \mapsto \mathbf{A}^{\mathcal{I}} = \{A_{ij}\}_{\forall i \notin \mathcal{I}, j} \cup \{A_{ij} = 0\}_{\forall i \in \mathcal{I}, j}$. This ensures that X_i for $i \in \mathcal{I}$ is independent of Z_j for all $j \neq i$. Note that in order for (6) to be able to approximate the interventional distribution in (3), an intervention on VACA should satisfy **Property 2**, i.e.:

Proposition 2. (*Causal interventions*). *VACA captures causal interventions if and only if the number of hidden layers in its decoder is greater than or equal to $\gamma - 1$, with γ being the length of the longest path between any two endogenous nodes in \mathcal{G} .*

To illustrate this, Figure 2 depicts how messages are exchanged in a one-hidden-layer decoder GNN corresponding to the causal graph \mathcal{G} in Figure 1 (*triangle* with $\gamma = 2$), both (a) without and (b) with an intervention on X_2 . We highlight in blue the direct messages (sent via direct causal path in \mathcal{G}), and in red the indirect messages (sent via indirect causal path in \mathcal{G}) from Z_1 to X_3 . Observe that, similarly to Figure 1, in (a) there is an indirect path (via h_2) from Z_1 to X_3 ; while in (b) this path is severed. Hence, the hidden layer (h_1, h_2, h_3) allows to distinguish between direct and indirect paths and thus to capture interventional effects. As the condition in Proposition 2 is more restrictive than the one in Proposition 1, VACA is able to approximate the observational and interventional distributions (as empirically validated in Appendix D) if:

Design condition 1 (necessary condition) *The decoder GNN of VACA has at least as many hidden layers as $\gamma - 1$, with γ being the longest directed path in the causal graph \mathcal{G} .*

4.3 Counterfactual distribution

VACA approximates the *counterfactual distribution* in (4) as (illustrated in Figure 3c):

$$p(\mathbf{x}^{CF} \mid do(\mathbf{X}_{\mathcal{I}} = \boldsymbol{\alpha}), \mathbf{x}^F) \approx \underbrace{\int \int p_{\theta}(\mathbf{X} \mid \tilde{\mathbf{Z}}^F, \tilde{\mathbf{Z}}^{\mathcal{I}}, \mathbf{A}^{\mathcal{I}}) q_{\phi}(\tilde{\mathbf{Z}}^{\mathcal{I}} \mid \mathbf{x}^{\mathcal{I}}, \mathbf{A}^{\mathcal{I}})}_{\text{action}} \underbrace{q_{\phi}(\tilde{\mathbf{Z}}^F \mid \mathbf{x}^F, \mathbf{A})}_{\text{abduction}} d\tilde{\mathbf{Z}}^{\mathcal{I}} d\tilde{\mathbf{Z}}^F}_{\text{prediction}}, \quad (7)$$

where \mathbf{x}^F represents a sample from \mathbf{X} for which we seek to compute the distribution over counterfactual \mathbf{x}^{CF} and $\tilde{\mathbf{Z}}^F = \{Z_i^F\}_{i \notin \mathcal{I}}$. Note that two different passes of the encoder are necessary: one for the *abduction* step of the factual instance $q_{\phi}(\tilde{\mathbf{Z}}^F \mid \mathbf{x}^F, \mathbf{A})$; and another one for the *action* step (intervention) $q_{\phi}(\tilde{\mathbf{Z}}^{\mathcal{I}} \mid \mathbf{x}^{\mathcal{I}}, \mathbf{A}^{\mathcal{I}})$ with $x_i^{\mathcal{I}} = \alpha_i \forall i \in \mathcal{I}$ (we remark that the rest of the values in $\mathbf{x}^{\mathcal{I}}$ do not affect the overall counterfactual computation).

We then evaluate the likelihood making sure that the resulting counterfactual sample \mathbf{x}^{CF} only depends on the $\tilde{\mathbf{Z}}^F$ and $\tilde{\mathbf{Z}}^{\mathcal{I}}$. Importantly, in order for VACA to be able to approximate the counterfactual distribution, we need its abduction (and action) step(s) to comply with **Property 3**, i.e.:

Proposition 3. (*Abduction*). *The abduction step of an observed sample $\mathbf{x} = \{x_1, \dots, x_d\}$ in VACA satisfies that for all i the posterior of Z_i is independent on the subset $\{x_j\}_{j \notin \text{pa}^*(i)} \subseteq \mathbf{x}$, if and only if the encoder GNN has no hidden layers.*

SCM	Model	Obs.	Interventional			Counterfactuals		Num. params	
		MMD	MMD	MeanE	StdE	MSE	SSE		
<i>collider</i>	LIN	MultiCVAE	30.37±8.16	44.70±12.25	13.29±4.78	46.56±2.40	87.41±3.64	65.15±2.83	553
		CAREFL	9.27±1.49	4.86±0.45	0.35±0.08	81.89±1.78	8.11±0.58	7.83±0.55	6420
		VACA	1.50±0.67	1.57±0.41	0.75±0.31	41.99±0.30	9.86±0.74	7.06±0.38	5600
	NLIN	MultiCVAE	28.03±9.12	41.60±12.62	10.49±4.12	46.48±2.43	82.32±2.61	62.05±1.87	553
		CAREFL	10.38±2.00	4.69±0.38	0.19±0.07	80.68±2.08	6.93±0.40	7.15±0.64	4308
		VACA	0.95±0.27	0.97±0.23	0.26±0.12	42.20±0.24	5.01±0.73	4.08±0.54	1805
<i>loan</i>	MultiCVAE	90.38±11.31	213.65±5.38	12.24±1.33	65.78±1.13	40.98±0.35	15.12±0.16	33717	
	CAREFL	22.10±1.64	27.38±4.07	6.74±4.25	50.13±2.47	11.15±2.57	6.59±0.38	2880	
	VACA	2.22±0.25	6.87±0.66	4.35±0.35	3.83±0.08	10.30±0.40	6.41±0.11	30402	
<i>adult</i>	MultiCVAE	140.15±6.37	155.52±5.93	12.18±2.36	63.52±4.05	39.96±0.36	16.37±0.65	6549	
	CAREFL	31.31±1.58	34.31±5.77	12.54±3.17	41.26±3.44	1.23±0.17	3.55±0.90	127420	
	VACA	4.51±0.45	12.68±1.95	1.65±0.23	3.37±0.09	5.33±0.27	5.67±0.20	63432	

Table 1: Performance of different methods at estimating the observational, interventional and counterfactual distribution of different complex SCMs. Values are multiplied by 100. All models have been cross-validated with a similar computational budget. The number of parameters of the best configuration is shown in the right column.

The above result (proved in Appendix B) can be shown by the message passing algorithm computed by the encoder GNN, and leads to the second design condition of VACA:

Design condition 2 (necessary condition): *The encoder GNN of VACA has no hidden layers.*

In other words, from the definition of the SCM, the posterior distribution of U_i only depends on the parents, i.e. $U_i \mid X_{\text{pa}(i)}$. In order for VACA to mimic this property, the GNN that parameterized the encoder contains no hidden layers: in the message passing algorithm, in the k -th iteration (layer), a node depends on its k -hop ancestors; requiring $k = 1$ in the encoder refers to a GNN without hidden layers. Note that while the above condition may look restrictive and limiting the capacity of our encoder, we may choose arbitrarily complex NNs for the message f^m and update f^u functions, as well as one or more aggregation functions f^a , e.g., sum or max, to model the encoder [4].

4.4 Practical considerations

Next, we briefly discuss practical implementation considerations to handle complex causal models, which often appear in real world applications [7, 6] For further details on VACA implementation, refer to Appendix C.

Heterogeneous causal nodes. So far, we have modeled each endogenous variable X_i as a node in the causal graph \mathcal{G} , and thus in the VACA GNNs. Yet, in some application domains the relationships between a subset of k_i variables may be unknown, or they may be affected by hidden confounders. In such cases, we assume that set of k_i variables to be correlated and model them as one multidimensional and potentially heterogeneous node $\mathbf{X}_i = \{X_{i1}, \dots, X_{ik_i}\}$ that share the same latent random variable Z_i . This allows us to deal with a large variety of graphs in practice.

Heterogeneous endogenous variables. Heterogeneous causal nodes require us to model different functions for each node, i.e. nodes may now contain a mix of continuous/discrete variables. In general GNNs are parametrized such that the parameters of the message function f^m and update function f^u are shared for all the nodes and edges in the graph. However, similar to the structural equations \mathbf{F} , we can define a unique set of parameters θ_{mij} for each f_{ij}^m (see (1)), so that we can model a different function for every edge in the causal graph. Further, we can also assume different update functions f_i^u for each node i , by introducing different update parameters θ_{ui} . Note, however, that VACA can be used with any GNN architecture [4, 15].

5 Evaluation

In this section, we evaluate the potential of VACA in approximating the outcomes of causal queries and compare it to two competing methods in synthetic experiments. The synthetic setting allows us to have access the true SEs, which is necessary to evaluate interventional distributions and especially counterfactuals. We consider interventions of the form $do(x_i = \alpha_i)$ for several values of α_i on both root and non-root nodes. We compute all results over the same 10 random seeds and report mean and standard deviation. Refer to Appendix E for a complete description of the experimental setup. Moreover, our code is publicly available at GitHub[†].

Datasets. We consider 6 different synthetic causal graphs that differ in the number of nodes d , diameter δ , and longest path γ . Here, we report the results for i) the *collider* ($d = 3$, $\delta = 1$, $\gamma = 1$) with linear (LIN) and non-linear (NLIN) additive noise SEs, ii) the

[†]<https://github.com/psanch21/VACA>

Metric	full	unaware	fair-x	fair-z
$\uparrow f1$	71.67	69.49	59.50	70.79 ± 5.15
$\downarrow uf$	14.01 ± 2.26	13.27 ± 2.28	0.14 ± 0.02	0.51 ± 0.19

Table 2: Counterfactual unfairness (uf) and f1-score ($f1$) of an SVM over 10 VACA seeds. Values multiplied by 100.

loan from Karimi et al. [16] ($d = 7, \delta = 2, \gamma = 3$), and iii) the *adult* ($d = 11, \delta = 2, \gamma = 3$) graphs. Note that the two latter ones are synthetic versions of the German Credit dataset [7] and the Adult datasets [6], respectively. See Appendix E.1 for further details on the graphs and Appendix E.4 for the results with the remaining graphs.

Metrics. We evaluate the observational distribution using the Maximum Mean Discrepancy (MMD) [13] as distance-measure between the true and estimated distributions, i.e., the lower the MMD the better the distributions match. For the interventional distribution, we additionally report the average estimation squared error of the mean (MeanE) and of the standard deviation (StdE) over all descendants of the intervened-upon variables. For the counterfactual distribution we report the mean squared error (MSE) as well as the standard deviation of the squared error (SSE) between the true and the estimated counterfactual value. More details in Appendix E.3.

Baselines. We compare VACA with MultiCVAE [16] and CAREFL [17] described in Section 1.1. For a fair comparison, all model hyperparameters have been cross-validated using a similar computational budget (see Appendix E.2). In Table 1, we report for each model and SCM the best configuration according to observational MMD. We also include a time-complexity analysis in Appendix E.5.

Results. Table 1 summarizes the results. We observe that, in general, MultiCVAE underperforms the other methods. This may be explained by the fact that MultiCVAE trains each node independently, and thus the discrepancy between the true and generated distributions in one node may be amplified in its descendants. Comparing VACA to CAREFL, we first observe that VACA performs consistently better in terms of observational MMD, i.e., VACA is able to generate observational samples that better resemble the true ones. Second, regarding the interventional distribution, CAREFL does a good job at fitting the mean (i.e., low MeanE). However, VACA performs consistently better both at approximating the standard deviation (i.e., low StdE) and the true samples (i.e., low MMD). This can be explained by VACA i) leveraging the causal graph (contrary to CAREFL that relies on causal ordering), and ii) optimizing the log-evidence in (5) jointly (contrary to the sequential optimization of MultiCVAE). Thus, VACA approximates the distribution as a whole better, which is a desirable property for studying interventions on a population-level rather than just on average. Lastly, in the approximation of counterfactuals we observe that both CAREFL and VACA exhibit similar performance in terms of MSE and SSE. Note however that CAREFL performs exact inference while VACA is built on approximate inference and is trained on a lower bound on the log-evidence. Finding tighter bounds could boost VACA performance.

6 Use case: counterfactual fairness

We finally show two practical use-cases of our method: assessing counterfactual fairness and training counterfactually fair classifiers. We use the public German Credit dataset [7] and rely on the causal model proposed by Chiappa [3] with the following random variables \mathbf{X} : sensitive feature $S = \{sex\}$, and non-sensitive features $C = \{age\}$, $R = \{credit\ amount, repayment\ history\}$ and $H = \{checking\ account, savings, housing\}$. Then, we aim to predict the binary feature $Y = \{credit\ risk\}$ from \mathbf{X} . See Appendix F for further details.

Counterfactual fairness. Let $S \subset \mathbf{X}$ be a sensitive attribute (e.g., gender), then the counterfactual unfairness [23] of a classifier $h : \mathbf{X} \rightarrow Y$ is measured $\forall \mathbf{x}^{CF}, \alpha' \neq \alpha, y$ as:

$$uf = | P(h(\mathbf{x}^{CF}) = y \mid do(S = \alpha), \mathbf{x}^F) - P(h(\mathbf{x}^{CF}) = y \mid do(S = \alpha'), \mathbf{x}^F) | \quad (8)$$

A classifier is counterfactually fair ($uf = 0$), if, given a factual \mathbf{x}^F with sensitive attribute $S = \alpha$, had its sensitive attribute been different $S = \alpha'$, the classifier prediction would remain the same. We can use VACA to generate counterfactual estimates to *audit* the fairness level of a classifier. Following [23], we *audit*: i) a *full* model $h_{full} : \mathbf{X} \rightarrow Y$ that takes as input the complete variable set; ii) an *unaware* model $h_{unaw} : \mathbf{X} \setminus S \rightarrow Y$ that takes as input all variables but the sensitive one; iii) and a *fair* model $h_{fair-x} : \{X_i \mid S \notin \text{an}^*(i)\} \rightarrow Y$ that takes as input all non-descendant variables of the sensitive attribute. Moreover, we show that we can *learn a fair classifier* $h_{fair-z} : \mathbf{Z} \setminus Z_S \rightarrow Y$, which takes as input the latent variables generated by the VACA encoder without the one of the sensitive attribute Z_S .

Fairness Auditing. Table 2 summarizes the unfairness level and f1-score for a support vector machine (SVM) classifier. See Appendix F for results of a logistic regression classifier. As we do not have access to the true data generation process, we evaluate the *auditing* task by the resulting ranking of the different classifiers according to their unfairness level. Based on the counterfactual generation by VACA the *full* classifier is consistently less fair than the *unaware* and the *fair-x* classifier, respectively. This ranking is consistent with the one in [23].

Fairness Classification Table 2 shows that for the *fair-x* classifier fairness comes at the expense of accuracy compared to the *full* classifier. On the contrary, even though VACA has been trained for representation learning without access to classification labels, *fair-z* is a fair classifier (with comparable fairness level to the *fair-x* one) while keeping the performance comparable to the unfair *full*

classifier. VACA, therefore, does not only allow us to audit counterfactual fairness but also provides a practical approach to train accurate and fair classifiers.

7 Conclusion, Limitations and Impact

In this work, we have proposed VACA, a variational causal autoencoder based on GNNs that: i) is specially designed to capture the properties of SCMs; ii) inherently handles heterogeneous data; and iii) provides good approximations of interventional and counterfactual distributions as a whole for SCMs of different complexities. As demonstrated by extensive synthetic experiments, VACA provides accurate results for a wide range of interventions in diverse SCMs leading to more consistent results than competing methods [16, 17]. Finally, we have applied VACA for counterfactually fair classification.

Practical limitations. The expressive power of VACA to model complex structural equations, e.g., in domains such as biology [37], is limited by the GNN architectures of the encoder and the decoder. As discussed in the GNN literature [4], especially aggregation functions may limit expressiveness. We expect VACA to benefit from advances in the field. Second, long causal paths would require VACA to increase the number of layers in the decoder (see **Design condition 1**). However, the GNNs performance is known to deteriorate with depth [9, 14, 24].

Social impact. Trusting counterfactuals is of great importance for decision making, e.g. in the political or medical domain. We thus encourage anyone who uses VACA (or any other ML method for causal inference) to i) fully understand the model assumptions and to verify (up to the possible extend) that they are fulfilled; as well as ii) to be aware of the identifiability problem in counterfactual queries [49, 45].

Future work. First, it would be important to evaluate the sensitivity of VACA to errors in the assumed causal graph, as well as to the presence of hidden confounders. We plan to extend VACA to handle more complex causal models including, e.g., hidden confounders and non-DAG causal graphs. Second, it would be interesting to perform ablation studies on the limitations of available GNNs architectures [44] for the VACA encoder and decoder; as well as on how the performance deteriorates as we increase the length of the causal path and thus the required number of hidden layers [24]. Finally, it would be intriguing to apply VACA to other causal questions recently discussed in the machine learning literature, such as privacy-preserving causal inference [22] or explainable machine learning [16].

Acknowledgments

We would like to thank Adrián Javaloy Bornás, Amir Hossein-Karimi, Jonas Kleesen and Maryam Meghdadi Esfahani for helpful feedback and discussions. Moreover, a special thanks to Diego Baptista Theuerkauf for invaluable help with formalizing proofs. Moreover, the authors would like to thank Ilyes Khemakhem for helpful insights in how to generalize their CAREFL approach to arbitrary graphs.

Pablo Sánchez Martín is supported by the German Research Foundation through the Cluster of Excellence “Machine Learning – New Perspectives for Science”, EXC 2064/1, project number 390727645. Miriam Rateike is supported by the German Federal Ministry of Education and Research (BMBF): Tübingen AI Center, FKZ: 01IS18039B. The authors thank for the generous funding support. The authors also thank the International Max Planck Research School for Intelligent Systems (IMPRS-IS) for supporting Pablo Sañchez Martín.

References

- [1] Jasmijn Bastings, Ivan Titov, Wilker Aziz, Diego Marcheggiani, and Khalil Sima'an. Graph convolutional encoders for syntax-aware neural machine translation. In *Proceedings of the Conference on Empirical Methods in Natural Language Processing (EMNLP)*, volume 3, 2017.
- [2] Yuri Burda, Roger Grosse, and Ruslan Salakhutdinov. Importance weighted autoencoders. In *Proceedings of the International Conference on Learning Representations (ICLR)*, volume 4, 2016.
- [3] Silvia Chiappa. Path-specific counterfactual fairness. In *Proceedings of the AAAI Conference on Artificial Intelligence*, volume 33, 2019.
- [4] Gabriele Corso, Luca Cavalleri, Dominique Beaini, Pietro Liò, and Petar Veličković. Principal neighbourhood aggregation for graph nets. In *Advances in Neural Information Processing Systems (NeurIPS)*, volume 33, 2020.
- [5] Austin Derrow-Pinion, Jennifer She, David Wong, Oliver Lange, Todd Hester, Luis Perez, Marc Nunkesser, Seongjae Lee, Xueying Guo, Brett Wiltshire, et al. Eta prediction with graph neural networks in google maps. *arXiv preprint arXiv:2108.11482*, 2021.
- [6] Dheeru Dua and Casey Graff. UCI machine learning repository, 2017. URL <https://archive.ics.uci.edu/ml/datasets/adult>.
- [7] Dheeru Dua and Casey Graff. UCI machine learning repository, 2017. URL [https://archive.ics.uci.edu/ml/datasets/statlog+\(german+credit+data\)](https://archive.ics.uci.edu/ml/datasets/statlog+(german+credit+data)).
- [8] Conor Durkan, Artur Bekasov, Iain Murray, and George Papamakarios. Neural spline flows. In *Advances in Neural Information Processing Systems*, volume 32, 2019.
- [9] Claudio Gallicchio and Alessio Micheli. Fast and deep graph neural networks. In *Proceedings of the AAAI Conference on Artificial Intelligence*, volume 34, 2020.
- [10] Sergio Garrido, Stanislav Borysov, Jeppe Rich, and Francisco Pereira. Estimating causal effects with the neural autoregressive density estimator. *Journal of Causal Inference*, 9, 2021.
- [11] Justin Gilmer, Samuel S Schoenholz, Patrick F Riley, Oriol Vinyals, and George E Dahl. Neural message passing for quantum chemistry. In *Proceedings of the International Conference on Machine Learning (ICML)*, volume 34. PMLR, 2017.
- [12] Clark Glymour, Kun Zhang, and Peter Spirtes. Review of causal discovery methods based on graphical models. *Frontiers in genetics*, 10:524, 2019.
- [13] Arthur Gretton, Karsten M Borgwardt, Malte J Rasch, Bernhard Schölkopf, and Alexander Smola. A kernel two-sample test. *The Journal of Machine Learning Research (JMLR)*, 13, 2012.
- [14] Fangda Gu, Heng Chang, Wenwu Zhu, Somayeh Sojoudi, and Laurent El Ghaoui. Implicit graph neural networks. In *Advances in Neural Information Processing Systems*, volume 33, 2020.
- [15] Will Hamilton, Zhitao Ying, and Jure Leskovec. Inductive representation learning on large graphs. In *Advances in Neural Information Processing Systems (NeurIPS)*, volume 30, 2017.
- [16] Amir-Hossein Karimi, Julius von Kügelgen, Bernhard Schölkopf, and Isabel Valera. Algorithmic recourse under imperfect causal knowledge: a probabilistic approach. In *Advances in Neural Information Processing Systems*, volume 33, pages 265–277, 2020.
- [17] Ilyes Khemakhem, Ricardo Monti, Robert Leech, and Aapo Hyvarinen. Causal autoregressive flows. In *Proceedings of International Conference on Artificial Intelligence and Statistics (AISTATS)*, volume 24. PMLR, 2021.
- [18] Hyemi Kim, Seungjae Shin, JoonHo Jang, Kyungwoo Song, Weonyoung Joo, Wanmo Kang, and Il-Chul Moon. Counterfactual fairness with disentangled causal effect variational autoencoder. In *Proceedings of the AAAI Conference on Artificial Intelligence*, volume 35, 2021.
- [19] Diederik P Kingma and Max Welling. Auto-encoding variational bayes. In *Proceedings of the International Conference on Learning Representations (ICLR)*, volume 2, 2014.
- [20] Thomas N Kipf and Max Welling. Variational graph auto-encoders. *arXiv preprint arXiv:1611.07308*, 2016.
- [21] Murat Kocaoglu, Christopher Snyder, Alexandros G. Dimakis, and Sriram Vishwanath. CausalGAN: Learning causal implicit generative models with adversarial training. In *Proceedings of the International Conference on Learning Representations (ICLR)*, volume 6, 2018.

- [22] Matt J Kusner, Yu Sun, Karthik Sridharan, and Kilian Q Weinberger. Private causal inference. In *Proceedings of the Conference on Artificial Intelligence and Statistics (AISTATS)*, volume 19. PMLR, 2016.
- [23] Matt J Kusner, Joshua Loftus, Chris Russell, and Ricardo Silva. Counterfactual fairness. In *Advances in Neural Information Processing Systems (NeurIPS)*, volume 30, 2017.
- [24] Qimai Li, Zhichao Han, and Xiao-Ming Wu. Deeper insights into graph convolutional networks for semi-supervised learning. In *Proceedings of the AAAI Conference on Artificial Intelligence*, volume 32, 2018.
- [25] Christos Louizos, Uri Shalit, Joris M Mooij, David Sontag, Richard Zemel, and Max Welling. Causal effect inference with deep latent-variable models. In *Advances in Neural Information Processing Systems (NeurIPS)*, volume 30, 2017.
- [26] Raha Moraffah, Bahman Moraffah, Mansooreh Karami, Adrienne Raglin, and Huan Liu. Can: A causal adversarial network for learning observational and interventional distributions. *arXiv preprint arXiv:2008.11376*, 2020.
- [27] Sebastian Nowozin. Debiasing evidence approximations: On importance-weighted autoencoders and jackknife variational inference. In *Proceedings of the International Conference on Learning Representations (ICML)*, volume 35. PMLR, 2018.
- [28] Álvaro Parafita and Jordi Vitrià. Explaining visual models by causal attribution. In *2019 IEEE/CVF International Conference on Computer Vision Workshop (ICCVW)*, pages 4167–4175. IEEE, 2019.
- [29] Álvaro Parafita and Jordi Vitrià. Causal inference with deep causal graphs. *arXiv preprint arXiv:2006.08380*, 2020.
- [30] Álvaro Parafita and Jordi Vitrià. Explaining visual models by causal attribution. In *International Conference on Computer Vision Workshop (ICCVW)*, 2019.
- [31] Nick Pawlowski, Daniel Coelho de Castro, and Ben Glocker. Deep structural causal models for tractable counterfactual inference. In *Advances in Neural Information Processing Systems (NeurIPS)*, volume 33, 2020.
- [32] Judea Pearl. Causal inference in statistics: An overview. *Statistics surveys*, 3, 2009.
- [33] Judea Pearl. *Causality*. Cambridge university press, 2009.
- [34] Jonas Peters, Dominik Janzing, and Bernhard Schölkopf. *Elements of causal inference: Foundations and learning algorithms*. The MIT Press, 2017.
- [35] Tom Rainforth, Adam Kosiorek, Tuan Anh Le, Chris Maddison, Maximilian Igl, Frank Wood, and Yee Whye Teh. Tighter variational bounds are not necessarily better. In *Proceedings of the International Conference on Machine Learning (ICML)*, volume 35. PMLR, 2018.
- [36] Vineeth Rakesh, Ruocheng Guo, Raha Moraffah, Nitin Agarwal, and Huan Liu. Linked causal variational autoencoder for inferring paired spillover effects. In *Proceedings of the International Conference on Information and Knowledge Management (CIKM)*. ACM, 2018.
- [37] Karen Sachs, Omar Perez, Dana Pe’er, Douglas A Lauffenburger, and Garry P Nolan. Causal protein-signaling networks derived from multiparameter single-cell data. *Science*, 308(5721):523–529, 2005.
- [38] Bernhard Schölkopf. Causality for machine learning. *arXiv preprint arXiv:1911.10500*, 2019.
- [39] Patrick Schwab, Lorenz Linhardt, and Walter Karlen. Perfect match: A simple method for learning representations for counterfactual inference with neural networks. *arXiv preprint arXiv:1810.00656*, 2018.
- [40] Xinwei Shen, Furu Liu, Hanze Dong, Qing Lian, Zhitang Chen, and Tong Zhang. Disentangled generative causal representation learning. *arXiv preprint arXiv:2010.02637*, 2020.
- [41] George Tucker, Dieterich Lawson, Shixiang Gu, and Chris J Maddison. Doubly reparameterized gradient estimators for monte carlo objectives. In *International Conference on Learning Representations*, 2018.
- [42] Matthew J Vowels, Necati Cihan Camgoz, and Richard Bowden. D’ya like dags? a survey on structure learning and causal discovery. *arXiv preprint arXiv:2103.02582*, 2021.
- [43] Matthew James Vowels, Necati Cihan Camgoz, and Richard Bowden. Targeted vae: Structured inference and targeted learning for causal parameter estimation. *arXiv preprint arXiv:2009.13472*, 2020.
- [44] Zonghan Wu, Shirui Pan, Fengwen Chen, Guodong Long, Chengqi Zhang, and S Yu Philip. A comprehensive survey on graph neural networks. *IEEE Transactions on Neural Networks and Learning Systems*, 2020.
- [45] Kevin Xia, Kai-Zhan Lee, Yoshua Bengio, and Elias Bareinboim. The causal-neural connection: Expressiveness, learnability, and inference. *arXiv preprint arXiv:2107.00793*, 2021.

- [46] Mengyue Yang, Furui Liu, Zhitang Chen, Xinwei Shen, Jianye Hao, and Jun Wang. Causalvae: Disentangled representation learning via neural structural causal models. *arXiv preprint arXiv:2004.08697*, 2020.
- [47] Bing Yu, Haoteng Yin, and Zhanxing Zhu. Spatio-temporal graph convolutional networks: a deep learning framework for traffic forecasting. In *Proceedings of the International Joint Conference on Artificial Intelligence (IJCAI)*, volume 27, 2018.
- [48] Yue Yu, Jie Chen, Tian Gao, and Mo Yu. Dag-gnn: Dag structure learning with graph neural networks. In *Proceedings of the International Conference on Machine Learning (ICML)*, volume 36. PMLR, 2019.
- [49] Matej Zečević, Devendra Singh Dhami, Petar Veličković, and Kristian Kersting. Relating graph neural networks to structural causal models. *arXiv preprint arXiv:2109.04173*, 2021.
- [50] Cheng Zhang, Kun Zhang, and Yingzhen Li. A causal view on robustness of neural networks. *Advances in Neural Information Processing Systems*, 33, 2020.
- [51] Muhan Zhang, Shali Jiang, Zhicheng Cui, Roman Garnett, and Yixin Chen. D-vae: A variational autoencoder for directed acyclic graphs. In *Advances in Neural Information Processing Systems (NeurIPS)*, volume 32, 2019.
- [52] Min Zheng and Samantha Kleinberg. Using domain knowledge to overcome latent variables in causal inference from time series. In *Proceedings of the Machine Learning for Healthcare Conference (MLHC)*. PMLR, 2019.

Algorithm 1: Message passing GNN with L layers decomposed in three operations

```

Input: A directed graph  $\mathcal{G}$  with  $d$  nodes, adjacency matrix  $\mathbf{A}$  and node features  $\mathbf{X}$ .
Output:  $\mathbf{H} = \{h_i^l\}_{i=1}^d$ .
 $h_i^0 = x_i \forall i$ 
for  $l = 1, \dots, L$ ; // For each layer  $l$ 
do
  for  $i = 1, \dots, d$ ; // For node  $i$ 
  do
     $m_{ij}^l = f^m(h_i^{l-1}, h_j^{l-1}; \theta_m^l) \forall j \in \mathcal{N}_i$ ; // Compute the messages
     $M_i^l = f^a(\{m_{ij}^l\}_{j \in \mathcal{N}_i})$ ; // Compute the aggregated message
     $h_i^l = f^u(h_i^{l-1}, M_i^l; \theta_u^l)$ ; // Compute the node features at layer  $l$ 
  end
end

```

A Background details on message passing Graph Neural Networks

A *directed graph* with $|\mathcal{V}| = d$ nodes can be represented as $\mathcal{G} := (\mathcal{V}, \mathcal{E})$, where \mathcal{V} denotes the set of nodes and $(j, i) \in \mathcal{E}$ is the set of directed edges from j to i . Additionally, we denote with $\mathbf{X} \in \mathbb{R}^{d \times F_X}$ the features of the nodes (the row index identifies the node, i.e., the i -th row contains the F_X -dimensional features of the node i). Also, the adjacency matrix $\mathbf{A} \in \{0, 1\}^{d \times d}$ of \mathcal{G} is defined as $A_{ij} = 1$ if there is an edge from j to i and $A_{ij} = 0$ otherwise. Then, a directed graph can be alternatively represented as $\mathcal{G} = (\mathbf{X}, \mathbf{A})$. Given a graph \mathcal{G} , a *Graph Neural Network (GNN) with parameters* θ is a function $f_\theta : \mathbb{R}^{d \times F_X} \times \{0, 1\}^{d \times d} \rightarrow \mathbb{R}^{d \times F_H}$ that takes into account the graph structure contained in the adjacency matrix $\mathbf{A} \in \{0, 1\}^{d \times d}$ and transforms the node features \mathbf{X} into different features $\mathbf{H} \in \mathbb{R}^{d \times F_H}$, i.e., $\mathbf{H} = f(\mathbf{X}, \mathbf{A}; \theta)$ (for readability we consider $f_\theta(\cdot) \equiv f(\cdot; \theta)$). Importantly, at the output of the GNN we have a graph (\mathbf{H}, \mathbf{A}) that preserves the structure of the input graph (\mathbf{X}, \mathbf{A}) .

A **GNN based on message passing** [11] is a type of spatial convolution GNNs [44] in which information is passed following the message passing process: In each layer l of the GNN each node i receives information from its neighbors \mathcal{N}_i , a.k.a. the parents of i . In a message passing GNN, the feature vector of the i -th node at the output of a layer l —i.e., h_i^l —is computed in three steps:

1. **Message**. The *message from node j to node i* is defined as $m_{ij}^l = f^m(h_i^{l-1}, h_j^{l-1}; \theta_m^l)$, where h_i^{l-1} are the features of node i at layer $l - 1$, h_j^{l-1} are the features of node j at the previous layer $l - 1$, and f^m is a neural network (usually a linear layer) parametrized by θ_m^l .
2. **Aggregator**. The *aggregator* is a function in charge of combining all the incoming messages at each node i into a single message, a.k.a. the aggregated message $M_i^l = f^a(\{m_{ij}^l \mid j \in \mathcal{N}_i\})$. Notice that f^a does not have any parameters. Choices of f^a may be the sum, mean, standard deviation, max or min over the inputs, i.e., messages [4].
3. **Update**. The *update function* $h_i^l = f^u(h_i^{l-1}, M_i^l; \theta_u^l)$ takes the aggregated message and the representation of node i at layer $l - 1$ and outputs the new representation for node i at layer l . The function f^u is defined as a neural network (usually a linear layer) with parameters θ_u^l .

Putting the three steps together, we obtain the general form of a message passing based GNN layer as $h_i^l = f^u(h_i^{l-1}, f^a(\{f^m(h_i^{l-1}, h_j^{l-1}; \theta_m^l) \mid j \in \mathcal{N}_i\}); \theta_u^l)$.

Algorithm 1 describes the propagation of information (i.e., messages) in a GNN with L layers.

B Proofs

For completeness, this section first formalizes the meaning of causal factorization, interventions and the abduction step in VACA.

VACA causal factorization refers to the factorization of the joint distribution as

$$p_\theta(\mathbf{X} \mid \mathbf{Z}, \mathbf{A}) = \prod_i p_{\theta_i}(X_i; \boldsymbol{\eta}_i),$$

where the likelihood parameters $\boldsymbol{\eta}_i = \boldsymbol{\eta}_i(\mathbf{Z}_{\text{an}^*(i)})$ are a function of all (and only) the features of the ancestors of i and the features of i .

A *VACA intervention* is performed by removing all the edges towards the intervened node i , such that $\mathcal{N}_i = \emptyset$, while the rest of the edges remains untouched.

In a VACA *abduction step*, the posterior distribution factorizes as

$$q_\phi(\mathbf{Z} \mid \mathbf{X}) = \prod_i q_{\phi_i}(Z_i; \boldsymbol{\eta}_i^{enc}),$$

where the distribution parameters $\boldsymbol{\eta}_i^{enc} = \boldsymbol{\eta}_i^{enc}(\mathbf{X}_{\text{pa}^*(i)})$ are a function of all (and only) the features of node i and the features of its the parents.

Notation. Consider a *causal graph* $\mathcal{G} := (\mathbf{X}, \mathbf{A})$, which is a directed acyclic graph (DAG). Let us define a path of length n from node u to node v in \mathcal{G} as $p(u, v) = (u, w_1, w_2, \dots, w_{n-1}, v)$, which is an ordered sequence of unique nodes such that i) there exists an edge in \mathcal{G} between concurrent nodes, ii) the first node is u , iii) and the last node is v . We refer to the length of the path as $|p(u, v)|$, i.e., the number of edges in the path, or alternatively, the number of nodes minus one. Let us define $P(u, v)$ as the set of unique paths connecting u to v . Let us define the *shortest path from u to v* as $p^-(u, v)$ (i.e. the path with the minimum number of edges to go from u to v) and its length as $d^-(u, v) = |p^-(u, v)|$. Let us define the *longest path from u to v* as $p^+(u, v)$ (i.e. the path with the maximum number of edges to go from u to v) and its length as $d^+(u, v) = |p^+(u, v)|$. Let us define the *set of ancestors of node i* (i.e., $\text{an}(i)$) as the set of nodes with paths to i , i.e., $\{j \mid |P(j, i)| > 0\}$. As for a GNN, we define the number of hidden layers (total number of layers minus one) as N_h .

Then, we define the *diameter* δ of the graph \mathcal{G} to be the length of the longest shortest path and γ to be the length of the longest path of the graph, which we compute as

$$\delta = \max_{u, v \in \mathcal{G}} d^-(u, v) \quad \text{and} \quad \gamma = \max_{u, v \in \mathcal{G}} d^+(u, v).$$

Lemma 1. *A message passing Graph Neural Network (GNN) has at least N_h hidden layers if and only if the output feature of every node i (i.e., $h_i^{N_h+1}$) receives information from any other node j via paths $p(j, i)$ such that $|p(j, i)| \leq N_h + 1$.*

Proof. Step 1. The statement is that the feature of every node i at the output of a GNN with N_h hidden layers (i.e., $h_i^{N_h+1}$) receives information from any other node j via paths $p(j, i)$ such that $|p(j, i)| \leq N_h + 1$. We give a proof by induction on N_h for an arbitrary node i , with input feature to the GNN h_i^0 and output feature $h_i^{N_h+1}$.

Base case: The statement holds for $N_h = 0$. By definition, a message passing GNN with one layer only exchanges messages between neighboring nodes. Hence, i) the output feature of node i is $h_i^1 = f(\{h_i^0\} \cup \{h_j^0 \mid j \in \mathcal{N}_i\}; \theta)$, which is only a function of the 1-hop ancestors (i.e., parents); ii) information is exchanged via paths that fulfill $|p(j, i)| \leq 1$.

Inductive step: We assume the statement holds for $N_h = k - 1$. In this case, i) the output feature of node i is $h_i^k = f(\{h_i^{k-1}\} \cup \{h_j^{k-1} \mid j \in \mathcal{N}_i\}; \theta)$, which is a function of the k -hop ancestors; ii) information is exchanged via paths that fulfill $|p(j, i)| \leq k$. For $N_h = k$, the output feature of node i is $h_i^{k+1} = f(\{h_i^k\} \cup \{h_j^k \mid j \in \mathcal{N}_i\}; \theta)$. Since h_j^k is a function of k -hop ancestors of node j , it follows that h_i^{k+1} is a function of the ancestors of h_j^k and on parents of node i , i.e., the output feature of node i is a function of its $(k + 1)$ -ancestors. Then, it follows that for $N_h = k$, information is exchanged via paths that fulfill $|p(j, i)| \leq k + 1$.

Step 2. We assume that the output feature of every node i receives information from any other node j via paths $p(j, i)$ such that $|p(j, i)| \leq N_h + 1$. Then, there exist node i and j such that $|p(j, i)| = N_h + 1$. Then, by definition, a message passing GNN needs at least N_h hidden layers to capture paths $p(j, i)$ with length $|p(j, i)| \leq N_h + 1$. \square

Remark. Lemma 1 implies that, for a given GNN with N_h hidden layers, the set of paths through which the output feature of node i is a function of node j is

$$P_{\text{GNN}}(j, i) = \{p(j, i) \mid p(j, i) \in P(j, i) \text{ and } |p(j, i)| \leq N_h + 1\}. \quad (9)$$

Additionally, if $|P_{\text{GNN}}(j, i)| = \emptyset$ then the output feature of node i is not a function of node j .

Proposition 1 (Causal factorization). *VACA satisfies causal factorization, $p_\theta(\mathbf{X} \mid \mathbf{Z}, \mathbf{A}) = \prod_i p_{\theta_i}(X_i \mid \mathbf{Z}_{\text{an}^*(i)})$, if and only if the number of hidden layers in the decoder is greater or equal than $\delta - 1$, with δ being the length of the longest shortest path between any two endogenous nodes.*

Proof. Consider a causal graph $\mathcal{G} := (\mathbf{X}, \mathbf{E})$ with diameter δ and a GNN decoder with N_h hidden layers. We assume VACA to satisfy causal factorization, i.e., $\boldsymbol{\eta}_i$ is a function $\mathbf{Z}_{\text{an}^*(i)}$ for all i . Therefore, there exist node i and j such that $d^-(j, i) = \delta$ (notice that this implies that j is an ancestor of i). Thus, by Lemma 1, the GNN decoder has $N_h \geq \delta - 1$ hidden layers. The converse is true because Lemma 1 is a bi-conditional statement. \square

Proposition 2 (Causal interventions). *VACA captures causal interventions if and only if the number of hidden layers in its decoder is greater than or equal to $\gamma - 1$, with γ being the length of the longest path between any two endogenous nodes in \mathcal{G} .*

N_h	<i>collider</i> ($\delta = 1, \gamma = 1$)		<i>triangle</i> ($\delta = 1, \gamma = 2$)		<i>chain</i> ($\delta = 2, \gamma = 2$)	
	MMD Obs. (%)	MMD Inter. (%)	MMD Obs. (%)	MMD Inter. (%)	MMD Obs. (%)	MMD Inter. (%)
0	1.86 \pm 0.84	1.16 \pm 0.86	21.76 \pm 5.80	48.47 \pm 12.57	9.69 \pm 1.92	17.24 \pm 2.82
1	1.31 \pm 0.36	0.75 \pm 0.17	9.17 \pm 2.39	19.91 \pm 4.75	6.44 \pm 1.52	10.36 \pm 2.67
2	1.32 \pm 0.41	1.09 \pm 1.08	7.19 \pm 3.14	14.10 \pm 6.45	4.35 \pm 1.77	6.55 \pm 1.64

Table 3: Evaluation of the observational and interventional distributions generated by VACA with different numbers of hidden layers N_h in the decoder. All metrics are multiplied by 100 (%).

A causal intervention involves to sever all the incoming edges to the intervened nodes. Thus, VACA can only capture causal interventions, if it can model all the causal paths, i.e., $P_{\text{GNN}}(j, i) = P(j, i) \forall i, j$. Otherwise, severing some paths will have no effect in the resulting intervention, as we prove next.

Proof. Consider a causal graph $\mathcal{G} := (\mathbf{X}, \mathbf{E})$ with length of the longest path between two nodes γ and a GNN decoder with N_h hidden layers. We assume that the GNN decoder models all the causal paths, i.e., $P_{\text{GNN}}(j, i) = P(j, i) \forall i, j$. By definition of γ , there exists at least one node i with an ancestor j such that $d^+(j, i) = \gamma$. Thus, by Lemma 1, the GNN decoder has $N_h \geq \gamma - 1$ hidden layers. The converse is true because Lemma 1 is a bi-conditional statement. \square

Proposition 3 (Abduction). *The abduction step of an observed sample $\mathbf{x} = \{x_1, \dots, x_d\}$ in VACA satisfies that for all i the posterior of Z_i is independent on the subset $\{x_j\}_{j \notin \text{pa}^*(i)} \subseteq \mathbf{x}$, if and only if the encoder GNN has no hidden layers.*

Proof. Consider a causal graph $\mathcal{G} := (\mathbf{X}, \mathbf{E})$ and a GNN encoder with N_h hidden layers. We assume the posterior of Z_i is independent on the subset $\{x_j\}_{j \notin \text{pa}^*(i)} \subseteq \mathbf{x}$, i.e., the parameters η_i^{enc} (the output of the GNN) is a function of $\{x_j\}_{j \in \text{pa}^*(i)}$. Then, the GNN only models paths $p(j, i)$ such that $d^+(j, i) = 1$. It follows, by Lemma 1, that the number of hidden layers of the encoder GNN is $N_h = 0$. The converse is true because Lemma 1 is a bi-conditional statement. \square

C VACA implementation details

In this section, we extend Section 4.4 and provide further details about the implementation of VACA for complex real-world datasets and causal graphs.

C.1 Heterogeneous endogenous variables

As described in Appendix A, each layer l of a GNN uses the same parameters $\theta = \{\theta_m^l, \theta_u^l\}$ (corresponding to f^m and f^u) to update the features of every node, i.e., $h_i^l = f(\{h_i^{l-1}\} \cup \{h_j^{l-1} \mid j \in \mathcal{N}_i\}; \theta)$ with f_θ being reused for all i . Nonetheless, the structural equations of an SCM define a unique function f_i for each node (see **Property 1**). To mimic this behavior, we will rely on *port numbering*. In particular, for a given causal graph \mathcal{G} , we uniquely identify each node with an index i and each edge with the pair of indexes of the nodes it connects.

Then, we define a *disjoint GNN layer* by the following characteristics:

- The node indexes define unique update functions f_i^u for each node, with parameters θ_{ui} .
- The edge indexes define unique message functions f_{ij}^m for each edge, with parameters θ_{mij} .

Consequently, parameters are not shared among nodes and we can mimic the diversity of the structural equations of an SCM and model heterogeneous endogenous variables. In our GitHub repository[‡], we present a PyTorch Geometric implementation of the *disjoint GNN layer*.

C.2 Heterogeneous causal nodes

Assume an SCM with d endogenous variables. As described in Section 4.4, is it possible to model an endogenous variable \mathbf{X}_i of the SCM as a heterogeneous node, i.e., $\mathbf{X}_i = \{X_{i1}, \dots, X_{ik_i}\}$, where k_i is the number of random variables in node i . In this section we describe the implications this has on the design of the encoder and decoder of VACA.

[‡]<https://github.com/psanch21/VACA>

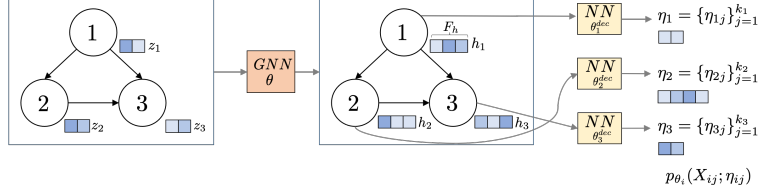


Figure 4: Heterogeneous VACA decoder architecture.

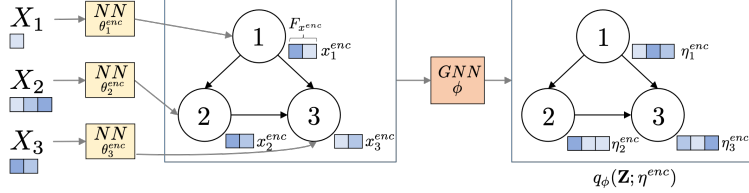


Figure 5: Heterogeneous VACA encoder architecture.

Implications for the decoder. Given the heterogeneous nature of the nodes, the likelihood of VACA factorizes as follows

$$p_{\theta}(\mathbf{X} | \mathbf{Z}) = \prod_{i=1}^d p_{\theta_i}(\mathbf{X}_i; \boldsymbol{\eta}_i) = \prod_{i=1}^d \prod_{j=1}^{k_i} p_{\theta_i}(X_{ij}; \boldsymbol{\eta}_{ij})$$

where $\boldsymbol{\eta}_i = \boldsymbol{\eta}_i(\mathbf{Z}_{\text{an}^*(i)})$ and $\boldsymbol{\eta}_{ij} = \boldsymbol{\eta}_{ij}(\mathbf{Z}_{\text{an}^*(i)})$.

Note, each $p(X_{ij}; \boldsymbol{\eta}_{ij})$ can be model with a different distribution, e.g., Gaussian or categorical. This means that the likelihood parameters $\boldsymbol{\eta}_{ij}$ for each random variable X_{ij} may be different depending on its distribution type. However, the decoder GNN transforms the latent features into different features $\mathbf{H} \in \mathbb{R}^{d \times F_h}$, where the feature vector of each node i has the same dimensionality F_h . As a consequence, \mathbf{H} cannot model the diversity in the likelihood parameters $\boldsymbol{\eta}_i$. To overcome such limitation, we add at the output of the GNN decoder a neural network (NN) per node i with parameters θ_i^{dec} . Such a NN transforms h_i , i.e. the output features of node i , into the set of likelihood parameters of each node $\boldsymbol{\eta}_i = \{\boldsymbol{\eta}_{ij}\}_{j=1}^{k_i}$, such that the likelihood parameters of each random variable $\boldsymbol{\eta}_{ij}$ satisfy the constraints of the corresponding likelihood $p(X_{ij}; \boldsymbol{\eta}_{ij})$ (e.g., non-negativity of variance for a Gaussian distribution). See Figure 4 for an illustration.

Implications for the encoder. Due to the heterogeneous nature of nodes, each endogenous variable $\mathbf{X}_i = \{X_{i1}, \dots, X_{ik_i}\}$, can have a different number of random variables k_i and thus the node i corresponding to it in the GNN will have features of different dimensions. However, as described in Appendix A, a GNN takes as input in general a matrix feature $\mathbf{X} \in \mathbb{R}^{d \times F_x^{\text{enc}}}$. This implies, the features of every node share the same dimensionality F_x^{enc} . To overcome this limitation, we include for each node i a neural network (NN) with parameters θ_i^{enc} that transforms the corresponding heterogeneous random variable \mathbf{X}_i into a feature vector with the dimension F_x^{enc} . See Figure 5 for an illustration.

D Validating & understanding VACA

Here, we empirically validate the design conditions of VACA and provide an analysis of the effect of the latent space dimension $\dim \mathbf{z}$ on the performance.

Validating VACA design conditions. In a first step we empirically validate our design choices for the VACA encoder and decoder. We show how the number of hidden layers N_h in the decoder affects the quality of the estimation of the observational and interventional distribution. We do so for three SCMs, with different values of longest shortest directed path δ and longest directed path γ . Our observations in Table 3 match our expectations. The *collider* ($\delta = \gamma = 1$) does not need any hidden layer to provide accurate estimate of both the observational and interventional distributions. In contrast, the *triangle* ($\delta = 1, \gamma = 2$) – in accordance with **Proposition 2** – needs at least one hidden layer to get a more accurate estimate of the interventional distribution. Finally, as stated by **Propositions 1** and **2**, the *chain* ($\delta = \gamma = 2$) requires at least one hidden layer to accurately approximate both the observational and interventional distributions.

Analysis of the latent space dimension. Here we present an analysis of the performance of VACA with respect to the dimension of the latent space $\dim \mathbf{z}$. Without loss of generality, we focus the analysis on the *collider*, *triangle* and *chain* graphs, and the NLIN and NADD structural equations. The results are depicted in Figure 6. All results are averaged over 10 different initializations. Regarding the observational distribution (left column), we observe that VACA overfits as we increase the $\dim \mathbf{z}$ for all SEMs and graphs under consideration. Specially, the performance degrades notoriously with $\dim \mathbf{z} = 32$. As shown in Table 4, the

dim z	<i>collider</i>		<i>triangle</i>		<i>chain</i>	
	NLIN	NADD	NLIN	NADD	NLIN	NADD
2	3785	3785	4542	4542	3785	3785
4	4445	4445	5334	5334	4445	4445
8	5765	5765	6918	6918	5765	5765
16	8405	8405	10086	10086	8405	8405
32	13685	13685	16422	16422	13685	13685

Table 4: Number of parameters of VACA for different dim z and datasets

number of parameters of VACA increases linearly with dim z . As for the interventional distribution (middle column), we observe similar behavior: for large values of dim z performance decreases and variance increases. For counterfactuals (right column), we observe a similar behavior but considerably less pronounced. In summary, we encourage practitioners to keep dim z small to avoid overfitting and obtain better and more consistent performance.

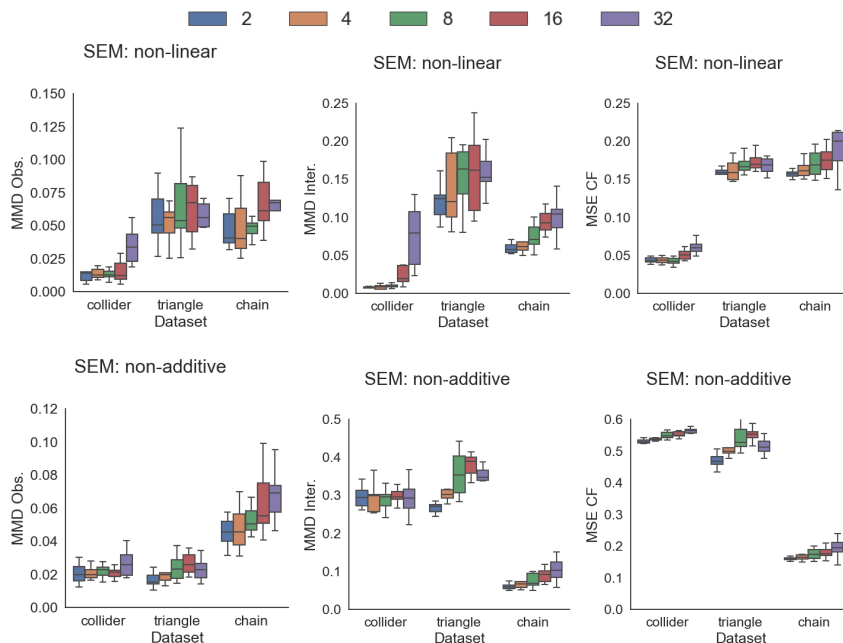


Figure 6: Performance of VACA varying the dimension of the latent space $\dim z \in \{2, 4, 8, 16, 32\}$ for the non-linear (top row) and non-additive (bottom row) SEMs of the *collider*, *triangle* and *chain* graphs. We evaluate the quality of the observational (MMD Obs.) (left column), interventional (MMD Inter.) (middle column), and counterfactual (MSE CF) (right column) distributions.

E Experiments: setting, metrics and further results

This section provides a complete description of the experimental set-up, including the (semi-)synthetic datasets (Section E.1), training of VACA, MultiCVAE [16] and CAREFL [17] (Section E.2), metrics reported in the experiments (Section E.3), additional results (Section E.4), complexity of the algorithm (Section E.5), and computing infrastructure (Section E.6).

E.1 Datasets

The following (semi-)synthetic datasets are taken from or inspired by [16]. The distribution of exogenous variables $p(\mathbf{U})$ for *triangle*, *chain* and *collider* follows Table 5 with MoG denoting a mixture of Gaussian distributions.

SCM	$p(U_1)$	$p(U_2)$	$p(U_3)$
LIN	MoG($0.5\mathcal{N}(-2, 1.5) + 0.5\mathcal{N}(1.5, 1)$)	$\mathcal{N}(0, 1)$	$\mathcal{N}(0, 1)$
NLIN	MoG($0.5\mathcal{N}(-2, 1.5) + 0.5\mathcal{N}(1.5, 1)$)	$\mathcal{N}(0, 0.1)$	$\mathcal{N}(0, 1)$
NADD	MoG($0.5\mathcal{N}(-2.5, 1) + 0.5\mathcal{N}(2.5, 1)$)	$\mathcal{N}(0, 0.25)$	$\mathcal{N}(0, 0.0625)$

Table 5: Distribution of exogenous variables $p(\mathbf{U})$ for SCM *triangle*, *chain*, *collider*.

	SCM	$\tilde{f}_1 := X_1$	$\tilde{f}_2 := X_2$	$\tilde{f}_3 := X_3$
<i>collider</i>	LIN	U_1	U_2	$0.05X_1 + 0.25X_2 + U_3$
	NLIN	U_1	U_2	$0.05X_1 + 0.25(X_2)^2 + U_3$
	NADD	U_1	U_2	$-1 + 0.1 \operatorname{sgn}(U_3)((X_1)^2 + (X_2)^2)U_3$
<i>triangle</i>	LIN	U_1	$-X_1 + U_2$	$X_1 + 0.25X_2 + U_3$
	NLIN	U_1	$-1 + \frac{3}{(1+\exp(-2X_1))} + U_2$	$X_1 + 0.25(X_2)^2 + U_3$
	NADD	U_1	$0.25 \operatorname{sgn}(U_2) * (X_1)^2(1 + (U_2)^2)$	$-1 + 0.1 \operatorname{sgn}(U_3)((X_1)^2 + (X_2)^2) + U_3$
<i>chain</i>	LIN	U_1	$-X_1 + U_2$	$0.25 * X_2 + U_3$
	NLIN	U_1	$-1 + \frac{3}{(1+\exp(-2X_1))} + U_2$	$0.25 * (X_2)^2 + U_3$
	NADD	U_1	$0.25 \operatorname{sgn}(U_2)(X_1)^2(1 + (U_2)^2)$	$-1 + 0.1 \operatorname{sgn}(U_3)((X_2)^2) + U_3$

Table 6: Structural equations $\tilde{\mathbf{F}}$ for different SCMs with $\mathbf{U} \sim p(\mathbf{U})$ in Table 5. Function $\operatorname{sgn}(x)$ returns an element-wise indication of the sign of x .

Collider. The *collider* is a synthetic dataset, which consists of 3 endogenous variables. The structural equations are shown in Table 6. Figure 7 illustrates the corresponding causal graph with $d = |\mathbf{X}| = 3$ nodes, diameter $\delta = 1$ and longest path $\gamma = 1$.

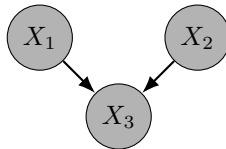


Figure 7: Causal graph for variables \mathbf{X} of SCM *collider*.

Triangle. The *triangle* is a synthetic dataset, which consists of 3 endogenous variables. The structural equations are shown in Table 6. Figure 8 illustrates the corresponding causal graph with $d = |\mathbf{X}| = 3$ nodes, diameter $\delta = 1$ and longest path $\gamma = 2$.

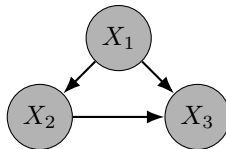


Figure 8: Causal graph for variables \mathbf{X} of SCM *triangle*.

Chain. The *chain* is a synthetic dataset, which consists of 3 endogenous variables. The structural equations are shown in Table 6. Figure 9 illustrates the corresponding causal graph with $d = |\mathbf{X}| = 3$ nodes, diameter $\delta = 2$ and longest path $\gamma = 2$.

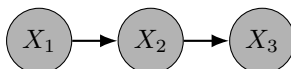


Figure 9: Causal graph for variables \mathbf{X} of SCM *chain*.

M-graph. The *M-graph* is a synthetic dataset, which consists of 5 endogenous variables. Here, the distributions of exogenous variables follow $U_i \sim p(U_i) = \mathcal{N}(0, 1) \forall i \in 1 \dots 5$. The structural equations are shown in Table 7 and Figure 10 illustrates the corresponding causal graph with $d = |\mathbf{X}| = 5$ nodes, diameter $\delta = 1$ and longest path $\gamma = 1$.

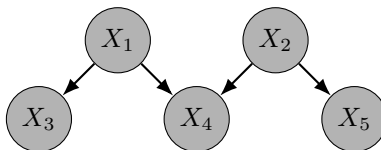


Figure 10: Causal graph for variables \mathbf{X} of SCM *M-graph*.

SCM	$\tilde{f}_1 := X_1$	$\tilde{f}_2 := X_2$	$\tilde{f}_3 := X_3$	$\tilde{f}_4 := X_4$	$\tilde{f}_5 := X_5$
LIN	U_1	U_2	$X_1 + U_3$	$-X_2 + 0.5X_1 + U_4$	$-1.5X_2 + U_5$
NLIN	U_1	U_2	$X_1 + 0.5(X_1)^2 + U_3$	$-X_2 + 0.5(X_1)^2 + U_4$	$-1.5(X_2)^2 + U_5$
NADD	U_1	U_2	$X_1 * U_3$	$(-X_2 + 0.5 * (X_1)^2)U_4$	$(-1.5(X_2)^2)U_5$

Table 7: Structural Equations $\tilde{\mathbf{F}}$ for SCM *M-graph* with $U_i \sim p(U_i) = \mathcal{N}(0, 1) \forall i \in 1 \dots 5$.

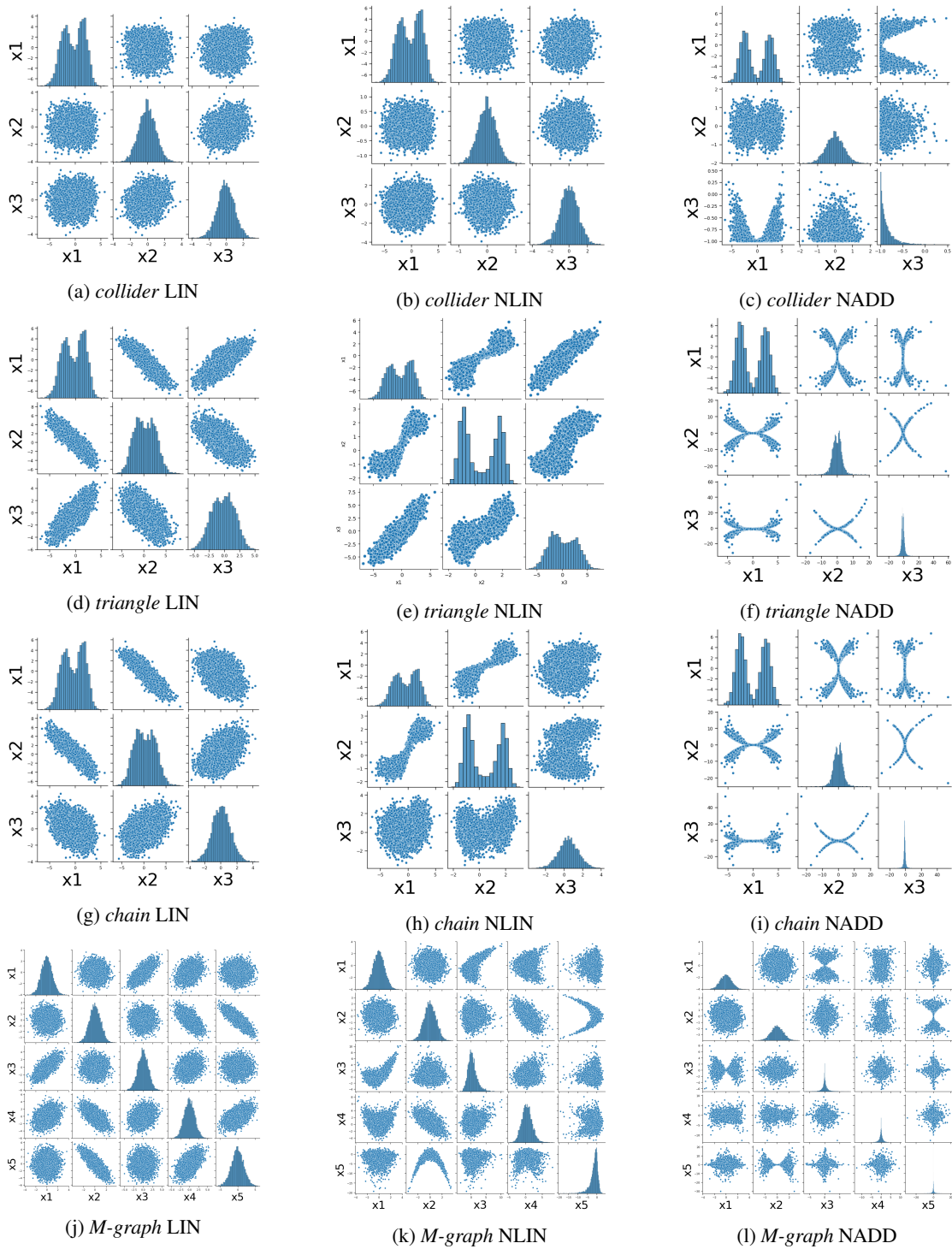


Figure 11: Histograms and scatter plots of pairwise feature relations for the *collider*, *triangle*, *chain* and *M-graph* datasets.

Loan. The *loan* is a semi-synthetic dataset from [16], which reflects a loan approval setting in the real-world inspired by German Credit dataset [7]. It consists of 7 endogenous variables: *gender G*, *age A*, *education E*, *loan amount L*, *loan duration D*, *income I* and *savings S* with the following structural equations and distributions of exogenous variables:

$$\begin{aligned}
 f_G : G &= U_G \\
 f_A : A &= -35 + U_A \\
 f_E : E &= -0.5 + \left(1 + e^{+1-0.5G-(1+e^{-0.1A})^{-1}-U_E}\right)^{-1} \\
 f_L : L &= 1 + 0.01(A - 5)(5 - A) + G + U_L \\
 f_D : D &= -1 + 0.1A + 2G + L + U_D \\
 f_I : I &= -4 + 0.1(A + 35) + 2G + GE + U_I \\
 f_S : S &= -4 + 1.5\mathbb{I}_{\{I>0\}}I + U_S
 \end{aligned}$$

with $U_G \sim \text{Bernoulli}(0.5)$, $U_A \sim \text{Gamma}(10, 3.5)$, $U_E \sim \mathcal{N}(0, 0.25)$, $U_L \sim \mathcal{N}(0, 4)$, $U_D \sim \mathcal{N}(0, 9)$, $U_S \sim \mathcal{N}(0, 25)$, $U_I \sim \mathcal{N}(0, 4)$.

Note, the authors model variables w.r.t. their relative meaning in terms of deviation from the mean. See [16] for further details. Figure 12 illustrates the corresponding causal graph with $d = |\mathbf{X}| = 7$ nodes, diameter $\delta = 2$ and longest path $\gamma = 3$.

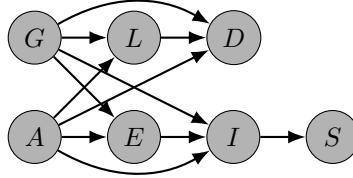


Figure 12: Causal graph for variables \mathbf{X} of SCM *loan*.

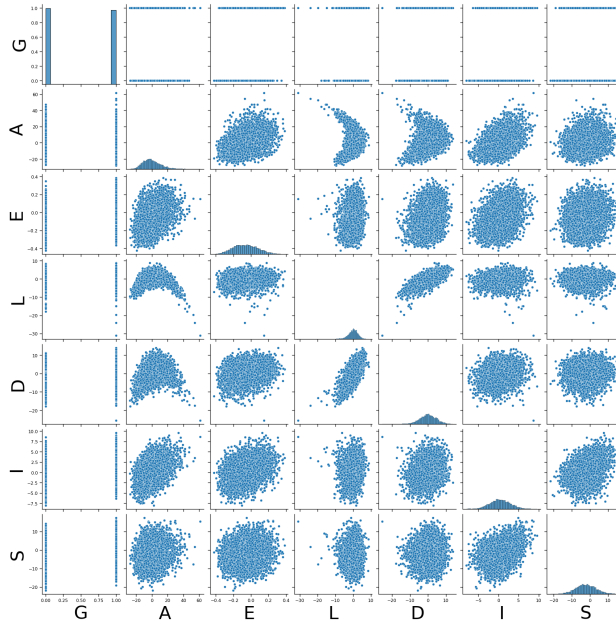


Figure 13: Histograms and scatter plots of pairwise feature relations for the *loan* dataset.

Adult. We introduce the new semi-synthetic *adult* dataset which aims to reflect the relationship between the variables that affect the annual income of a person inspired by the real-world Adult dataset [6]. Figure 15 shows the corresponding causal graph with $d = |\mathbf{X}| = 11$ nodes, diameter $\delta = 2$ and longest path $\gamma = 6$. We base the causal graph on [3]. Our dataset consists of the following 11 endogenous variables:

- *Race* R is an independent value.
- *Age* A is an independent value.
- *Native country* (N) is an independent value.
- *Sex* S is an independent value.
- *Education* level (E) depends on the sex, the native county and the race.
- *Hours (worked) per week* H depends additionally on the race, the native country and the sex. We consider this continuous variable to be between 0 and 80 hours.
- *Work status* W , i.e., being unemployed or self-employed, is a discrete variable that depends on the number of hours worked per day, age, native country, and level of education.
- *Marital status* M , i.e., married never married or separated, depends on age, race, work status, hours per week, native country and sex. Individuals under a certain age are never married.
- *Occupation* sector O is a discrete variable with values technology, social sciences and medicine. It depends on the race, age, education, marital status and sex.
- *Relationship status* L is a discrete variable, with values wife, own-child, husband, not-in-family, unmarried. It depends on marital status, education, age, native country, and sex.
- *Income* I depends on race, age, education, occupation, work status, marital status, hours per week, relationship status, native country, and sex.

These aspects are reflected in the following structural equations :

$$\begin{aligned}
f_R : R &= U_R & a_2 &= 2\mathbb{I}_{\{a_1 \in (20,40]\}} + \mathbb{I}_{\{a_1 \in (40,50]\}} + 2\mathbb{I}_{\{a_1 \geq 50\}} \\
f_A : A &= U_A + 17 & a_1 &= A + 2U_M \\
f_N : N &= U_N & h_2 &= h_1 \mathbb{I}_{\{h_1 \leq 2\}} + 2\mathbb{I}_{\{h_1 > 2\}} \\
f_S : S &= U_S & h_1 &= 3 \text{int}(\sigma(H - 30)) \\
f_E : E &= \exp(2\mathbb{I}_{\{R=0\}} + \mathbb{I}_{\{R=1\}}) + \sigma(A - 30) & f_L : L &= 0\mathbb{I}_{\{(M=1) \wedge (c < -1)\}} + 1\mathbb{I}_{\{(M=1) \wedge (c \geq -1)\}} \\
&+ (0.5\mathbb{I}_{\{S=0\}} + \mathbb{I}_{\{S=1\}})(2\mathbb{I}_{\{N=1\}} + 5\mathbb{I}_{\{N=2\}} & &+ 2\mathbb{I}_{\{(M \neq 1) \wedge (c \geq -1)\}} + 1\mathbb{I}_{\{(M \neq 1) \wedge (c < -1)\}} \\
&+ \mathbb{I}_{\{N=3\}}) + U_E & c &= c_n + c_e + 2\mathbb{I}_{\{A < 20\}} - 2\mathbb{I}_{\{S=0\}} \\
f_H : H &= ((40\mathbb{I}_{\{N=0\}} + 36\mathbb{I}_{\{N=1\}} + 50\mathbb{I}_{\{N=2\}} & c_n &= U_O \mathbb{I}_{\{N=0\}} - U_O \mathbb{I}_{\{N=1\}} + 2U_O \mathbb{I}_{\{N=2\}} + 2\mathbb{I}_{\{N=3\}} \\
&+ 30\mathbb{I}_{\{N=3\}}) * (0.5\mathbb{I}_{\{R=0\}} + \mathbb{I}_{\{R=1\}} + 1.3\mathbb{I}_{\{R=2\}}) & c_e &= \sigma(E - 30) \\
&+ 2 \exp(-(A - 30)^2) + 5 | \tanh(E - 2) | & f_O : O &= 0\mathbb{I}_{\{k < 1\}} + 1\mathbb{I}_{\{1 \leq k \leq 4\}} + 2\mathbb{I}_{\{4 < k\}} \\
&+ 2\mathbb{I}_{\{S=0\}} + U_H \mathbb{I}_{\{A < 70\}} & k &= R + k_a + k_e + W + 3M + 4S \\
f_W : W &= w_2 \mathbb{I}_{\{w_2 > 0\}}, & k_a &= 2e^{-(A+U_O-20)^2} \\
w_2 &= w_1 \mathbb{I}_{\{w_1 \leq 3\}} + 3\mathbb{I}_{\{w_1 > 3\}} & k_e &= -\sigma(E * U_O - 30) \\
w_1 &= \mathbb{I}_{\{5|\tanh(E-2)| + \sigma(H-30+U_W) > 0.3\}} & f_I : I &= U_I \\
&+ \mathbb{I}_{\{\sigma(H-30+U_W) > 0.3\}} \mathbb{I}_{\{(A+1.5U_W) > 50\}} & &+ 10,000\mathbb{I}_{\{R > 1.5\}} + 20,000\mathbb{I}_{\{R < 1.5\}} \\
&- \mathbb{I}_{\{N=0\}} + \mathbb{I}_{\{N=2\}} + 3\mathbb{I}_{\{N=3\}}) & &+ 3,000\mathbb{I}_{\{21 \leq A < 30\}} + 8,000\mathbb{I}_{\{30 \leq A\}} \\
f_M : M &= \text{mode}(r_2, a_2, W, h_2, H, g_3) & &+ 5,000\mathbb{I}_{\{E < 2\}} + 10,000\mathbb{I}_{\{2 \leq E < 10\}} + 30,000\mathbb{I}_{\{10 \leq E\}} \\
r_2 &= 2 * \mathbb{I}_{\{r_1=1\}} + \mathbb{I}_{\{r_1=2\}} & &+ 5,000\mathbb{I}_{\{O=1\}} + 15,000\mathbb{I}_{\{O=2\}} \\
r_1 &= \text{int}(R + 0.2U_M) \mathbb{I}_{\{R \in [0,2]\}} + 2\mathbb{I}_{\{R > 2\}} & &+ 5,000\mathbb{I}_{\{W=0\}} + 7,000\mathbb{I}_{\{W=1\}} \\
g_3 &= \mathbb{I}_{\{g_2=0\}} + 2 * \mathbb{I}_{\{g_2=1\}} & &+ 1,000\mathbb{I}_{\{M=0\}} + 4,000\mathbb{I}_{\{M=1\}} - 2,000\mathbb{I}_{\{M=2\}} \\
g_2 &= 0 * \mathbb{I}_{\{g_1 < 0\}} + \mathbb{I}_{\{g_1 > 1\}} + g_1 \mathbb{I}_{\{g_1 \in [0,1]\}} & &+ 15,000\mathbb{I}_{\{H > 45\}} + 10,000\mathbb{I}_{\{N \geq 2\}} \\
g_1 &= \text{int}(G + 0.5U_M) & &+ 4,000\mathbb{I}_{\{S=1\}} + 3,000\mathbb{I}_{\{R \leq 1\}}
\end{aligned}$$

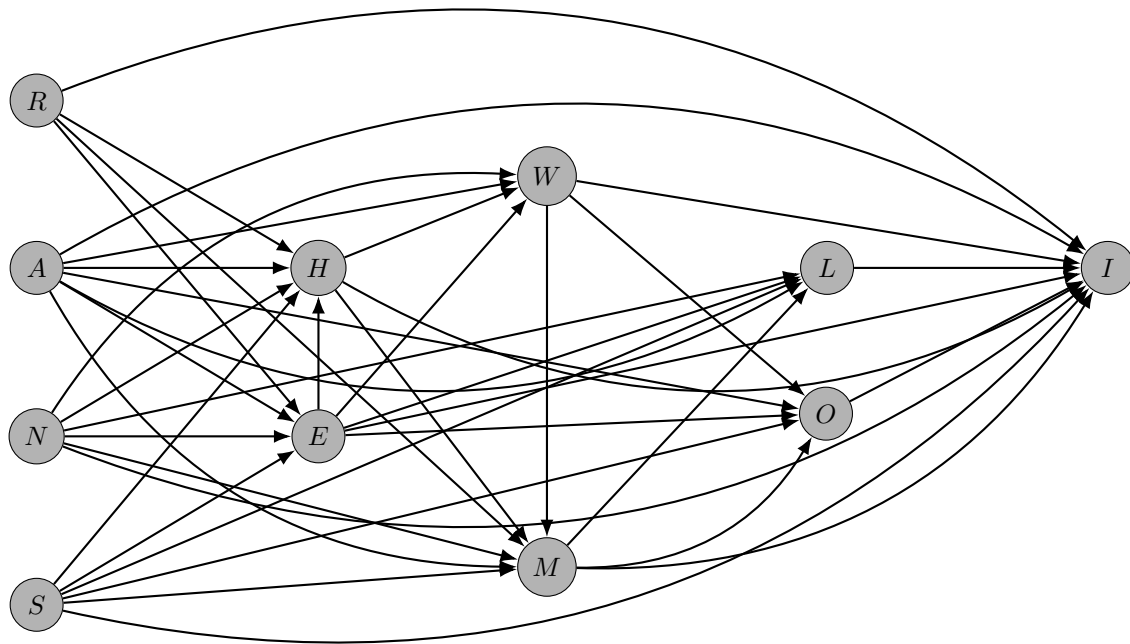


Figure 15: Causal graph for variables \mathbf{X} of SCM *adult*.

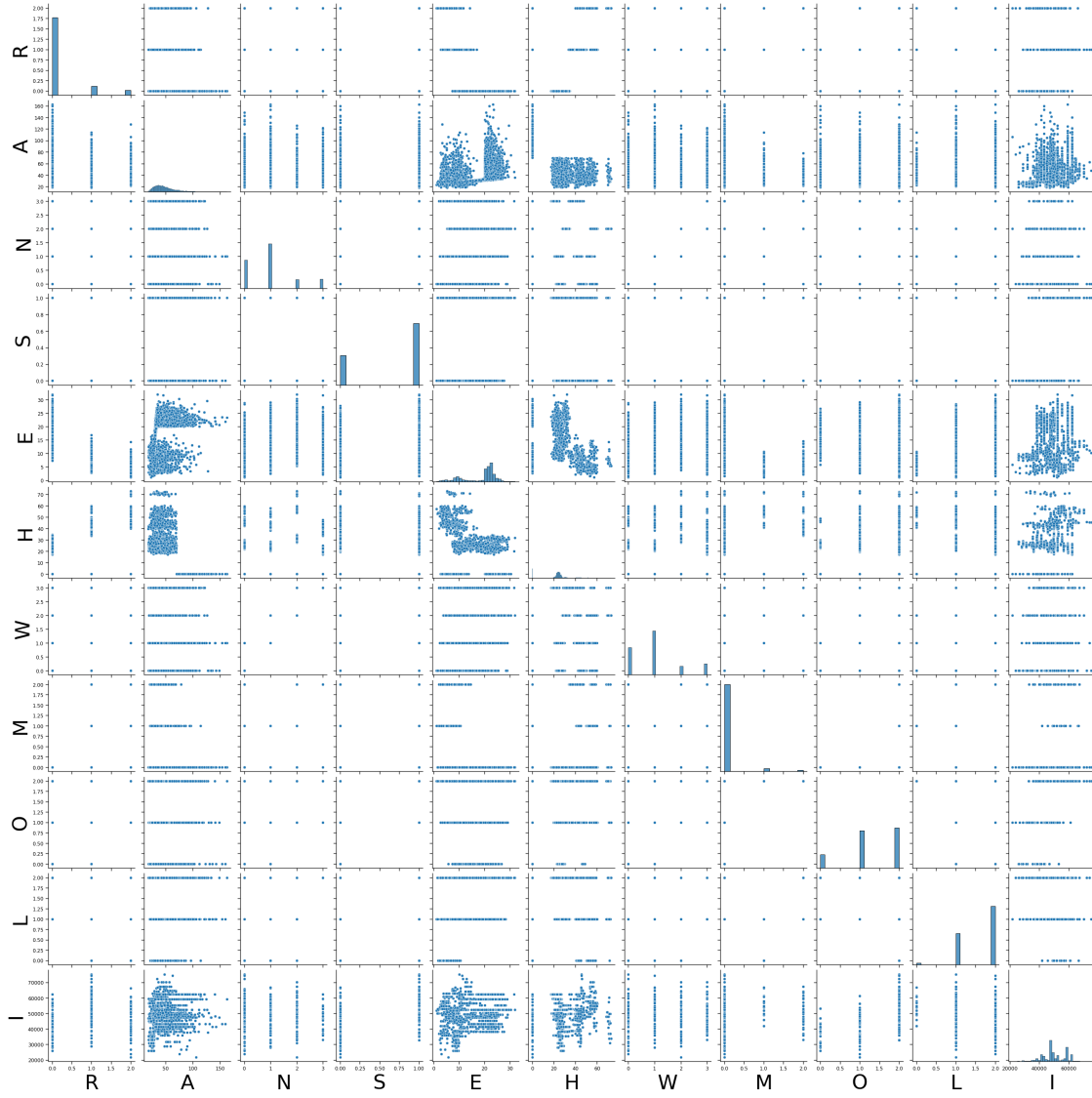


Figure 16: Histograms and scatter plots of pairwise feature relations for the *adult* dataset.

E.2 Training and cross-validation

This section details the hyperparameter cross-validation of VACA, MultiCVAE [16] and CAREFL [17] for the experiments in Tables 1 and Table 12. Across experiments and models we generate synthetic datasets consisting of 5000 training samples, 2500 test samples and 2500 validation samples and we use a batch size of 1000. All the models have been cross-validated using a similar computational budget, i.e. the number of combinations of hyperparameters cross-validated is the same for all the models (see Table 8). Additionally, we run each configuration over 10 different random initializations. Regarding the number of iterations, we assumed a large enough number of epochs for training loss to converge, and implemented early stopping to prevent overfitting the training data. The best configuration has been chosen in terms of the best observational MMD.

SCM	MultiCVAE	CAREFL	VACA
<i>chain</i>	72	72	72
<i>collider</i>	72	72	72
<i>triangle</i>	72	72	72
<i>M-graph</i>	72	72	72
<i>loan</i>	40	24	24

Table 8: Number of combinations of hyperparameters cross-validated for each of the models and datasets. Note that for each combination we run 10 different seeds.

VACA. We optimize the ELBO [19] and use the IWAE [2] with $K = 100$ as the objective metric for the early stopping procedure. We use the Rectified Linear Unit (ReLU) as activation function. We trained with a learning rate $\eta = 0.005$ for a maximum of 500 epochs, or alternatively until the objective metric does not improve in 50 epochs. Also, we regularize the training of VACA using a novel *parents dropout*: randomly removing all incoming edges to the nodes with probability $p \in [0, 1)$. In our experiments, we observe that adding this regularization improves overall performance. We cross-validated the parents dropout rate with values $\{0.1, 0.2\}$, the number of hidden layers of the decoder with values $\{0, 1, 2, 3, 4, 5\}$ (the specific values depend on the diameter of the graph) with 16 neurons each, and whether to use or not residual connections. The best models are reported in Table 9. We use a latent variable dimension of 4 and a Gaussian likelihood with a small variance $\sigma^2 = \lambda_{KLD}/2$ with $\lambda_{KLD} = 0.05$.

SCM		Encoder Arch.	Decoder Arch.	Parents Dropout	Residual
<i>chain</i>	LIN	$1 \times 16 \times 4$	$4 \times 16 \times 1$	0.1	1
	NLIN	$1 \times 16 \times 4$	$4 \times 16 \times 16 \times 1$	0.1	0
	NADD	$1 \times 16 \times 4$	$4 \times 64 \times 1$	0.1	1
<i>collider</i>	LIN	$1 \times 16 \times 4$	$4 \times 16 \times 16 \times 1$	0.2	1
	NLIN	$1 \times 16 \times 4$	$4 \times 16 \times 1$	0.1	0
	NADD	$1 \times 16 \times 4$	$4 \times 16 \times 16 \times 1$	0.1	1
<i>triangle</i>	LIN	$1 \times 16 \times 4$	$4 \times 16 \times 16 \times 1$	0.1	0
	NLIN	$1 \times 16 \times 4$	$4 \times 16 \times 16 \times 1$	0.2	0
	NADD	$1 \times 16 \times 4$	$4 \times 16 \times 16 \times 1$	0.1	0
<i>M-graph</i>	LIN	$1 \times 16 \times 4$	$4 \times 16 \times 1$	0.1	0
	NLIN	$1 \times 16 \times 4$	$4 \times 16 \times 16 \times 1$	0.1	0
	NADD	$1 \times 16 \times 4$	$4 \times 16 \times 16 \times 1$	0.1	0
<i>loan</i>	-	$1 \times 16 \times 16 \times 4$	$4 \times 16 \times 16 \times 16 \times 1$	0.1 2	0
<i>adult</i>	-	$1 \times 16 \times 16 \times 4$	$4 \times 8 \times 8 \times 8 \times 8 \times 1$	0.2	1

Table 9: Hyperparameter selection for our VACA training for the SCMs on the synthetic datasets *triangle*, *collider*, *chain* and *M-graph* and on the semi-synthetic dataset *loan*. Note, the encoder architecture refers to the layers in function f^m , while the decoder architecture refers to the different GNN layers.

MultiCVAE. Karimi et al. [16] propose to train a conditional variational autoencoder (CVAE) for each endogenous variable that is not a root node in the causal graph, we refer to as MultiCVAE. Different from [16], our implementation also models non-root nodes as CVAEs, since our goal is to model the joint distribution, while [16] target interventional and counterfactual distributions for algorithmic recourse only. Additionally, we perform the necessary modifications for training on normalized data.

SCM		λ_{KLD}	Encoder Arch.	Decoder Arch.	Dropout rate
<i>chain</i>	LIN	0.05	$1 \times 16 \times 4$	$4 \times 128 \times 1$	0.0
	NLIN	0.05	$1 \times 16 \times 1$	$1 \times 128 \times 1$	0.0
	NADD	0.05	$1 \times 16 \times 4$	$4 \times 128 \times 1$	0.0
<i>collider</i>	LIN	0.05	$1 \times 16 \times 4$	4×1	0.0
	NLIN	0.05	$1 \times 16 \times 4$	4×1	0.0
	NADD	0.05	$1 \times 16 \times 4$	4×1	0.0
<i>triangle</i>	LIN	0.05	$1 \times 16 \times 4$	$4 \times 128 \times 1$	0.2
	NLIN	0.05	$1 \times 16 \times 1$	$1 \times 128 \times 1$	0.1
	NADD	0.05	$1 \times 16 \times 4$	$4 \times 128 \times 1$	0.2
<i>M-graph</i>	LIN	0.05	$1 \times 16 \times 4$	4×1	0.2
	NLIN	0.05	$1 \times 16 \times 4$	4×1	0.1
	NADD	0.05	$1 \times 16 \times 4$	$4 \times 32 \times 32 \times 1$	0.2
<i>loan</i>	-	0.05	$1 \times 16 \times 16 \times 1$	$1 \times 64 \times 64 \times 1$	0.0
<i>adult</i>	-	0.05	$1 \times 16 \times 16 \times 2$	$2 \times 16 \times 1$	0.0

Table 10: Hyperparameter selection for MultiCVAE [16] training for the SCMs on the synthetic datasets with three nodes (i.e., *triangle*, *collider* and *chain*), *M-graph* and for the semi-synthetic dataset *loan*.

SCM		Flows	Hidden Units
<i>chain</i>	LIN	4	5
	NLIN	3	64
	NADD	5	5
<i>collider</i>	LIN	2	96
	NLIN	2	64
	NADD	3	16
<i>triangle</i>	LIN	4	64
	NLIN	4	5
	NADD	3	96
<i>M-graph</i>	LIN	4	64
	NLIN	4	96
	NADD	5	96
<i>loan</i>	-	4	64
<i>adult</i>	-	2	96

Table 11: Hyperparameter selection for CAREFL [17] training for different SCMs.

We cross-validated the number and size of hidden layers of the decoder, the dropout rate, and the dimension of the latent space. The best models (according to the observational MMD) are reported in Table 10. As with VACA, we assume $\lambda_{\text{KLD}} = 0.05$ for all SCMs and CVAEs.

CAREFL. Khemakhem et al. [17] propose CAREFL, an autoregressive causal flows model for causal discovery, which also allows to answer interventional and counterfactual queries. The authors rely on real-valued non-volume preserving (real NVP) transformations, since they mainly focus on the multivariate bi-variate case. As this flow architecture is not suited for general graphs, we use their framework with Neural Spline Autoregressive Flows [8]. We have cross validated the number of flows $\{2, 3, 4, 5, 6\}$ and the number of hidden units of the neural networks $\{5, 10, 16, 32, 64, 96\}$. The final configuration—i.e., the configuration with the lowest observational MMD—is displayed in Table 11.

E.3 Performance metrics

In the following we describe the metrics used to evaluate the performance of VACA in Section 5. In all experiments we use (semi-)synthetic datasets with access to samples from the ground truth distribution $\{\mathbf{x}_i\}_{i=0}^n \sim P$ as well as from the estimated distribution $\{\hat{\mathbf{x}}_i\}_{i=0}^n \sim Q$.

For the interventional and counterfactual distribution, we perform a set of interventions $\mathcal{I} = \{do(\mathbf{X}_{\mathcal{I}_j} = \alpha_j)\}_j$, where $\mathcal{I}_j \in [d]$ and $\alpha_j \in \{-1.0, -0.5, 0.0, 0.5, 1.0\} \times \sigma_{\mathcal{I}_j}$ with $\sigma_{\mathcal{I}_j}$ as the empirical standard deviation of the intervened variable $\mathbf{X}_{\mathcal{I}_j}$ prior to intervention (i.e., in the observational distribution). Note that we only intervene on one variable at a time. For each intervention in \mathcal{I} , we are interested in the estimated distribution of variables causally affected by the intervention $\{\mathbf{X}_i | i \in des(\mathcal{I}_j)\}$, i.e., the set of descendants of the variable intervened. Note that $des(\mathcal{I}_j)$ refers to the set of indexes of the descendants. It follows that we do not intervene on leaf nodes.

Mean Maximum Discrepancy (MMD). The Mean Maximum Discrepancy (MMD) [13] is a kernel-based distance-measure between two distributions P and Q on the basis of samples from both distributions. The smaller the MMD, the more likely it is that the sets of samples are drawn from the same distributions, i.e. the better distributions match.

Without access to underlying distribution, we can compute an unbiased empirical squared MMD estimate using a kernel function k as[13]:

$$\widehat{\text{MMD}}^2(\mathbf{X}, \hat{\mathbf{X}}) = \frac{1}{n(n-1)} \left(\sum_{i=1}^n \sum_{j=1}^n k(\mathbf{x}_i, \mathbf{x}_j) + \sum_{i=1}^n \sum_{j=1}^n k(\hat{\mathbf{x}}_i, \hat{\mathbf{x}}_j) - 2 \sum_{i=1}^n \sum_{j=1}^n k(\mathbf{x}_i, \hat{\mathbf{x}}_j) \right). \quad (10)$$

In our implementation we use as kernel a mixture of RBF (Gaussian) kernels with different bandwidths and sample size $n = 1000$.

Estimation squared error for the mean (MeanE). For the interventional distribution, we compute the estimation squared error for the mean (MeanE) as the average (across interventions) of the squared difference between the empirical means of the true and estimated interventional distributions (for the descendants of the intervened variables):

$$\text{MeanE} = \frac{1}{|\mathcal{I}|} \sum_{\mathcal{I}_j \in \mathcal{I}} \frac{1}{|des(\mathcal{I}_j)|} \sum_{i \in des(\mathcal{I}_j)} \left(E[X_i^{\mathcal{I}_j}] - E[\hat{X}_i^{\mathcal{I}_j}] \right)^2$$

Estimation squared error for the standard deviation (StdE). For the interventional distribution, we compute the estimation squared error for the standard deviation (StdE) as the average (across interventions) of the squared difference between the empirical standard deviation of the true $\tilde{\sigma}(X_i^{\mathcal{I}_j})$ and estimated $\tilde{\sigma}(\hat{X}_i^{\mathcal{I}_j})$ interventional distributions (for the descendants of the intervened variables):

$$\text{StdE} = \frac{1}{|\mathcal{I}|} \sum_{\mathcal{I}_j \in \mathcal{I}} \frac{1}{|des(\mathcal{I}_j)|} \sum_{i \in des(\mathcal{I}_j)} \left(\tilde{\sigma}(X_i^{\mathcal{I}_j}) - \tilde{\sigma}(\hat{X}_i^{\mathcal{I}_j}) \right)^2$$

Mean squared error (MSE). For the counterfactual distribution, we compute the mean squared error (MSE) as the average (across interventions) of the pairwise squared difference between true and estimated counterfactual values for the descendants of the intervened variable. More in detail, let us define the random variable $T^{\mathcal{I}_j}$ as the *Frobenius norm* of the difference between true $\mathbf{x}_{des(\mathcal{I}_j)}^{CF}$ and estimated $\hat{\mathbf{x}}_{des(\mathcal{I}_j)}^{CF}$ counterfactual values for the descendants of the intervened variable, i.e.,

$$T^{\mathcal{I}_j} = \|\mathbf{x}_{des(\mathcal{I}_j)}^{CF} - \hat{\mathbf{x}}_{des(\mathcal{I}_j)}^{CF}\|_2^2, \quad (11)$$

Thus, we can compute the counterfactual MSE as:

$$\text{MSE} = \frac{1}{|\mathcal{I}|} \sum_{\mathcal{I}_j \in \mathcal{I}} \frac{1}{|des(\mathcal{I}_j)|} E \left[T^{\mathcal{I}_j} \right] \quad (12)$$

Standard deviation of the squared error (SSE). Similarly, we can compute the average (across interventions) of the standard deviation of the counterfactual squared error as:

$$\text{SSE} = \frac{1}{|\mathcal{I}|} \sum_{\mathcal{I}_j \in \mathcal{I}} \frac{1}{|des(\mathcal{I}_j)|} \sum_{i \in des(\mathcal{I}_j)} \tilde{\sigma} \left(T^{\mathcal{I}_j} \right), \quad (13)$$

where $\tilde{\sigma}(T^{\mathcal{I}_j})$ denotes the empirical standard deviation of $T^{\mathcal{I}_j}$.

E.4 Additional results

In the following we present additional results that empirically show the potential of VACA to model interventional and counterfactual queries. In particular, we report the results for the *triangle*, *M-graph*, and *chain* graphs. We remark that the following results are consistent with the ones reported in the main manuscript for the *collider*, *loan* and *adult*.

SCM	Model	Obs.	Interventional		Counterfactuals			Num. params	
		MMD	MMD	MeanE	StdE	MSE	SSE		
collider	LIN	MultiCVAE	30.37±8.16	44.70±12.25	13.29±4.78	46.56±2.40	87.41±3.64	65.15±2.83	553
		CAREFL	9.27±1.49	4.86±0.45	0.35±0.08	81.89±1.78	8.11±0.58	7.83±0.55	6420
		VACA	1.50±0.67	1.57±0.41	0.75±0.31	41.99±0.30	9.86±0.74	7.06±0.38	5600
	NLIN	MultiCVAE	28.03±9.12	41.60±12.62	10.49±4.12	46.48±2.43	82.32±2.61	62.05±1.87	553
		CAREFL	10.38±2.00	4.69±0.38	0.19±0.07	80.68±2.08	6.93±0.40	7.15±0.64	4308
		VACA	0.95±0.27	0.97±0.23	0.26±0.12	42.20±0.24	5.01±0.73	4.08±0.54	1805
	NADD	MultiCVAE	29.72±8.90	117.67±46.20	26.23±11.09	39.75±1.34	73.93±10.44	51.44±6.06	553
		CAREFL	9.79±1.29	9.13±1.45	1.58±0.94	102.13±3.16	9.92±0.51	32.66±0.86	1710
		VACA	1.71±0.48	29.87±1.94	10.71±1.05	50.25±0.87	31.99±0.84	39.10±0.67	5600
triangle	LIN	MultiCVAE	33.12±3.89	157.50±15.08	12.10±2.03	44.66±2.57	65.95±3.05	42.39±1.75	3243
		CAREFL	13.50±1.83	8.88±0.54	0.62±0.25	80.11±2.44	7.05±1.09	8.91±1.43	8616
		VACA	3.64±1.64	13.82±1.87	2.90±0.49	25.82±0.33	23.52±1.83	16.02±1.32	5334
	NLIN	MultiCVAE	46.65±9.05	218.23±30.38	17.50±4.85	27.55±1.98	52.34±4.50	32.45±2.22	1785
		CAREFL	13.55±2.25	19.01±1.05	1.61±0.44	103.03±2.26	9.38±4.21	10.38±4.20	828
		VACA	6.04±1.87	9.53±3.60	1.44±0.59	17.93±0.19	13.24±1.93	8.26±1.29	5334
	NADD	MultiCVAE	16.99±7.22	133.83±16.96	2.59±3.38	18.25±0.83	42.43±0.87	20.55±1.15	3243
		CAREFL	13.58±1.69	74.51±14.18	1.31±0.84	148.03±6.96	11.62±1.50	53.71±0.98	9630
		VACA	1.72±0.67	30.10±4.41	0.19±0.14	26.64±1.30	22.50±2.61	41.16±3.91	5334
M-graph	LIN	MultiCVAE	38.60±4.06	80.89±20.73	25.82±6.26	17.73±3.39	54.72±4.71	27.47±2.28	933
		CAREFL	19.55±3.48	15.38±0.75	0.77±0.23	68.32±1.35	6.94±0.23	9.97±0.15	18200
		VACA	1.76±0.34	4.60±0.81	1.86±0.23	11.79±0.11	12.83±0.69	9.10±0.51	3249
	NLIN	MultiCVAE	37.95±6.21	84.79±18.15	24.97±9.10	16.66±3.28	51.30±5.24	25.90±1.23	933
		CAREFL	20.72±2.78	18.63±1.36	2.57±0.69	74.41±1.02	9.43±0.34	24.94±0.31	27160
		VACA	1.95±0.40	6.78±0.95	2.27±0.41	12.55±0.43	16.26±0.95	17.65±1.12	8001
	NADD	MultiCVAE	19.97±5.03	80.25±14.12	0.92±0.60	32.94±1.77	38.28±1.00	32.61±1.11	7277
		CAREFL	19.36±1.59	18.37±0.78	0.28±0.09	79.71±2.30	32.66±0.31	49.78±0.19	33950
		VACA	3.06±0.84	17.80±1.78	0.09±0.05	21.22±0.56	41.06±0.31	48.39±0.35	8001
chain	LIN	MultiCVAE	29.38±2.96	131.24±12.04	6.75±1.66	38.96±2.17	59.15±1.61	41.37±1.07	3099
		CAREFL	11.70±1.46	12.00±1.23	0.98±0.38	81.15±2.55	9.90±1.42	11.72±1.80	828
		VACA	4.47±0.72	5.73±1.11	3.60±0.62	22.91±0.23	23.09±1.18	15.77±0.77	5648
	NLIN	MultiCVAE	30.33±4.53	159.00±11.81	8.68±4.51	43.49±2.91	60.34±1.87	40.88±1.08	1641
		CAREFL	12.35±2.03	11.08±1.02	1.04±0.43	79.06±2.16	10.56±0.74	12.05±1.17	6462
		VACA	4.66±1.06	6.17±1.24	3.69±0.46	22.41±0.45	23.17±2.04	15.69±1.25	4445
	NADD	MultiCVAE	29.65±2.89	132.74±11.58	7.10±1.75	40.59±2.23	59.21±1.66	41.26±1.08	3099
		CAREFL	11.24±1.41	10.86±1.04	1.15±0.32	80.26±2.52	10.18±2.11	12.92±2.86	1035
		VACA	4.67±0.91	6.09±1.16	3.98±0.72	23.14±0.20	23.58±1.33	15.96±0.81	5648
loan	MultiCVAE	90.38±11.31	213.65±5.38	12.24±1.33	65.78±1.13	40.98±0.35	15.12±0.16	33717	
	CAREFL	22.10±1.64	27.38±4.07	6.74±4.25	50.13±2.47	11.15±2.57	6.59±0.38	2880	
	VACA	2.22±0.25	6.87±0.66	4.35±0.35	3.83±0.08	10.30±0.40	6.41±0.11	30402	
adult	MultiCVAE	140.15±6.37	155.52±5.93	12.18±2.36	63.52±4.05	39.96±0.36	16.37±0.65	6549	
	CAREFL	31.31±1.58	34.31±5.77	12.54±3.17	41.26±3.44	1.23±0.17	3.55±0.90	127420	
	VACA	4.51±0.45	12.68±1.95	1.65±0.23	3.37±0.09	5.33±0.27	5.67±0.20	63432	

Table 12: Performance of different methods at estimating the observational, interventional and counterfactual of different SCMs. All metrics are multiplied by 100.

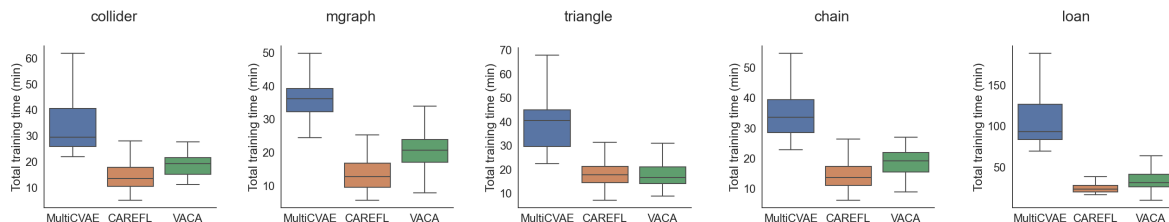


Figure 17: Training time (in minutes) for MultiCVAE, CAREFL and VACA for the different graphs.

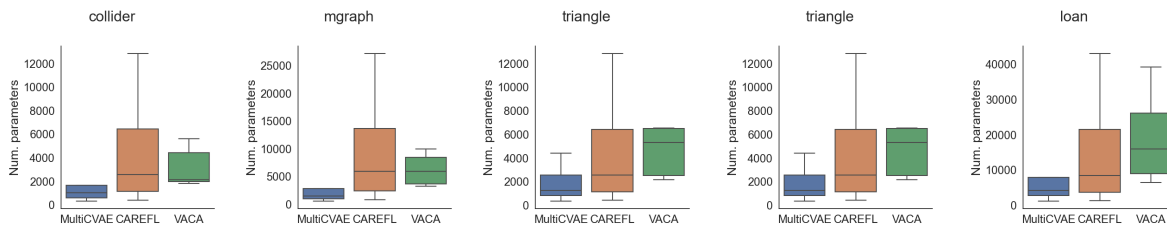


Figure 18: Number of parameters of MultiCVAE, CAREFL and VACA for the different graphs.

Results for interventional distributions. Table 12 (middle columns) reports the MMD, MeanE, and StdE for the interventional distribution. In accordance with the results shown in the main manuscript, we can observe that i) VACA consistently outperforms other methods in terms of MMD; ii) the three methods provide comparable results in capturing the mean of the interventional distribution (MeanE); and iii) CAREFL and MultiCVAE often fail to capture the standard deviation of the interventional distribution (StdE), while VACA provides a more accurate estimate of the overall interventional distribution (as can be easily seen in the MMD).

Results for the counterfactuals. Table 12 also reports the results for the counterfactual distribution, in terms of MSE and SSE. As reported in the main text, we observe that CAREFL provides more accurate estimates than VACA and MultiCVAE in terms of MSE, which may be explained by the fact that CAREFL performs exact inference as opposed to the approximated inference of the other two approaches. However, CAREFL presents high variance in its results (see SSE). In contrast, VACA leads to regularly lower values of SSE, which suggests more consistent counterfactual estimations across factual samples and interventions.

E.5 Complexity analysis

In this section we compare the amount of time that it takes VACA and the two baselines to converge during training. Figure 17 shows the time (in minutes) it takes to train the models for the configurations of hyperparameters cross-validated (see Section E.2). Note we also show the results averaged over 10 different initializations. We can extract three main points from Figure 17. Firstly, we observe that most of the experiments take less than 60 minutes to converge, only some experiments with the *loan* graph take longer. Secondly, MultiCVAE takes longer to converge than CAREFL and VACA on average. This can be explained by the fact that nodes of the graph are trained sequentially. Thirdly, we observe that CAREFL and VACA take similar amount of time to converge on average. We remark that experiments were run in a computer cluster, whose performance depends on its congestion, i.e. the number of people using the cluster and the amount of experiments. Thus, it is possible that part of the variance in the times is due to different congestion situations in the cluster.

Figure 18 shows a box-plot of the number of parameters of the configuration of hyperparameters cross-validated for the models and the datasets under study. Firstly, we observe that the configurations chosen for MultiCVAE contain less number of parameters than the configurations of the other two methods. However, increasing the number of parameters leads to an increase in training time. MultiCVAE already has the longest training time compared to the other methods, so the comparison is unfair in terms of time complexity. Regarding CAREFL and VACA, we observe that the number of parameters cross-validated overlaps in all the cases.

E.6 Computing infrastructure

All the experiments conducted in this work were executed in the same computer cluster based on the Linux OS. Each experiment was assigned to 2 CPUs (they could be assigned only to 1 CPU but the more CPUs, the faster the data-loading process is) and 8GB of memory. For information about the required software packages please refer to the official GitHub repository of VACA <https://github.com/psanch21/VACA>.

F Further details on the counterfactual fairness use-case

In this section we provide further details on dataset, training, metrics and additional results for the use-case of counterfactual fairness in Section 6.

F.1 German Credit Dataset

The German Credit dataset from the UCI repository [7] contains 20 attributes from 1000 loan applicants. We rely on the causal model proposed by in [3] for the following subset of features as exogenous variables \mathbf{X} (see Figure 19): sensitive feature $S = \{sex\}$, and non-sensitive features $C = \{age\}$, $R = \{credit\ amount, repayment\ history\}$ and $H = \{checking\ account, savings, housing\}$. The causal graph in Figure 19 has a diameter $\delta = 1$ and longest path $\gamma = 1$. The goal of a classifier h is to predict $Y = \{creditrisk\}$ from \mathbf{X} . We load and pre-process the data using the `aif360` library such that the dataset contains binary outcome variable Y (0-bad, 1-good) and a binary sensitive attribute S (0-female, 1-male). Note that the dataset contains 700 labels $Y = 1$ and 300

labels $Y = 0$, i.e., it is imbalanced. It also contains 690 males $S = 1$ and 310 females $Y = 0$. Note also that the causal model contains heterogeneous causal nodes (R and S), as addressed in Section 4.4. For example, [3] assume that the relationship between *credit amount* and *repayment history* is unknown, or that it may be affected by hidden confounders. This leads to an undirected path between the random variables and they are grouped together in one multidimensional causal node R . This applies similarly to node S .

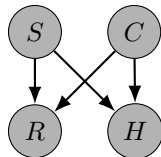


Figure 19: Causal graph for variables X of the German Credit dataset [3]

F.2 Training

In this section we provide further information on training VACA on the German Credit dataset [7] and detail the different classifiers in Section 6. We use a 80% training, 10% validation, 10% training data split.

VACA. Training for VACA was performed on normalized data—performing normalization only on the continuous variables, i.e. r.v. C and R in Fig 19. We trained a heterogeneous VACA as described in Section with a message passing function f^m with one hidden layer of 16 neurons, a decoder with one hidden layer of 16 neurons and a latent variable with dimension 4. We trained the model using the PIWAE [35] approach with $\lambda_{KLD} = 0.05$, specifically, the encoder with the IWAE [2] objective with $K = 5$ and the decoder with a β -ELBO with $\beta = 0.5$. We use a parents dropout rate (see Appendix E.2) of 0.2, learning rate of 0.005 and batch size 100.

Classifiers. Logistic Regression (LR) and Support Vector Machine (SVM) classifiers are taken from the scikit-learn library and trained with default parameters as well as `class_weight = balanced` due to the class imbalance of the dataset.

Metr.	CLF	full	unaware	fair-x	fair-z
↑ <i>acc</i>	LR	61.00	62.00	43.00	63.60 ± 4.74
	SVM	66.00	64.00	51.00	64.20 ± 4.52
↑ <i>f1</i>	LR	67.23	68.33	47.71	70.89 ± 4.11
	SVM	71.67	69.49	59.50	70.79 ± 5.15
↓ <i>uf</i>	LR	18.30 ± 3.22	17.65 ± 3.20	0.16 ± 0.02	0.44 ± 0.24
	SVM	14.01 ± 2.26	13.27 ± 2.28	0.14 ± 0.02	0.51 ± 0.19

Table 13: Counterfactual unfairness (*uf*), accuracy (*acc*) and f1-score (*f1*) of a LR and SVM classifier over 10 VACA seeds. Values multiplied by 100.

F.3 Metrics

In this section we detail the measures f1-score (f1), unfairness (uf) and accuracy (acc) in Table 13.

f1-score. Due to class imbalance, we measure classifier performance with the f1-score. The f1-score is the weighted average of the precision and recall and can assume values between 0 and 1; the higher the values the better. Our implementation relies on the `f1_score` from the scikit-learn library. We compute in expectation over our training dataset:

$$f1 = \mathbb{E} \left[2 \times \frac{\text{precision} \times \text{recall}}{\text{precision} + \text{recall}} \right]. \quad (14)$$

where precision is the ratio $\frac{TP}{TP+FP}$ with the number of true positives *TP* and the number of false positives *FP* and recall is the ratio $\frac{TP}{TP+FN}$ with the number of false positives *FP*.

Counterfactual (un)fairness. We measure counterfactual unfairness [23] with counterfactual instances \mathbf{x}^{CF} and classifier prediction $h(\mathbf{x}^{CF}) = \hat{y}^{CF}$ as expectation over our training dataset:

$$uf = \mathbb{E} \left[\left| p(y^F = 1 | \mathbf{x}^F) - p(\hat{y}^{CF} = 1 | do(S = a'), \mathbf{x}^F) \right| \right] \quad (15)$$

where $a' = 1 - a$ as $S \in \{0, 1\}$.

Accuracy. In Table 13, we report additionally the prediction accuracy as performance measure of classifier *h* with respect to factials (samples) (\mathbf{x}^F, y^F) and prediction $h(\mathbf{x}^F) = \hat{y}^F$ in expectation over our training dataset:

$$acc = \mathbb{E} \left[\mathbb{1} \left(y_i^F = \hat{y}_i^F \right) \right]. \quad (16)$$

Our implementation relies the `accuracy_score` from the scikit-learn library.